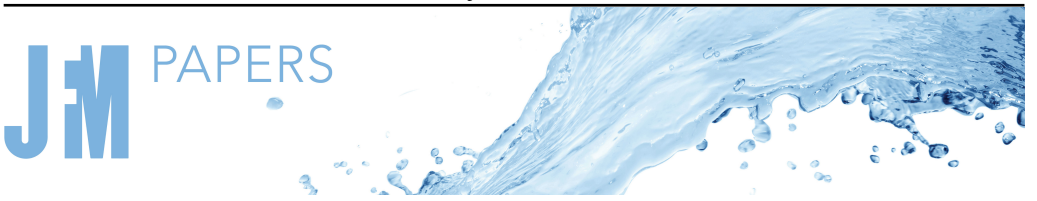
J. Fluid Mech. (2026), *vol.* 1039, A43, doi:10.1017/jfm.2026.11819



A double emulsion droplet in a two-directional shear flow

Moshe Favelukis

Department of Chemical Engineering, Shenkar – College of Engineering and Design, Ramat-Gan, 5252626, Israel

Corresponding author: Moshe Favelukis, favelukis@gmail.com

(Received 8 October 2025 UTC; revised 12 February 2026 UTC; accepted 19 June 2026 UTC)

This theoretical report explores a double emulsion droplet in a two-directional shear creeping flow. The droplet consists of a spherical inner drop (fluid 3) enclosed by a spherical shell (fluid 2), all immersed in external fluid 1. Six parameters govern: the capillary number (Ca), two viscosity ratios (λ_{21}, λ_{31}), the radii ratio (κ), the surface tensions ratio (Ω) and the flow-type (G). Using Lamb's solution, an analytical solution for the spherical case ($Ca = 0$, $\Omega = \infty$) was found. We explored small deformations with: $\lambda_{21} = O(1)$, $\lambda_{31} = O(1)$, $G = O(1)$, $Ca \ll 1$ and $Ca/\Omega \ll 1$. If $G > -1$, the outer surface is oriented at $\phi = +45°$, while the inner surface at $\phi = -45°$. The reverse occurs for $G < -1$. If $G = -1$, no deformation is possible. For a highly viscous shell ($\lambda_{21} \gg 1$), the deformation of the outer surface is independent of Ca and oriented at $\phi = 0°$ or $\phi = 90°$, while the deformation of the inner surface depends on Ca and at $\phi = \pm 45°$. The opposite occurs for highly viscous inner drop ($\lambda_{31} \gg 1$). Two breakup mechanisms were identified: contact between inner and outer surfaces, and inner drop rupture. Finally, we considered the effective viscosity of a dilute emulsion, containing spherical double emulsion droplets. In a single drop ($\kappa \to 0$), Taylor's expression is recovered. For a highly viscous or thin shell ($\lambda_{21} \to \infty$, $\kappa \to 1$), Einstein's formula is obtained.

Key words: low-Reynolds-number flows, drops and bubbles

1. Introduction

Double emulsion droplets have received much attention in the fluid mechanics literature as they offer many more potential applications when compared with single drops. Several arrangements can be considered as a double emulsion droplet and the one in this report is made up from a spherical drop, fully engulfed by a spherical fluid shell. This structure,

© The Author(s), 2026. Published by Cambridge University Press.

https://doi.org/10.1017/jfm.2026.11819 Published online by Cambridge University Press

also named a compound drop, a globule or an encapsulated droplet, can be found in the pharmaceutical, food and cosmetic industries. There, useful materials are protected in the inner drop and, if wanted, can be later released, in a control form, to the external ambient fluid. Other applications involving double emulsion droplets are: direct contact heat exchangers, liquid membrane separations and biological cell modelling, just to name a few. A good starting point, on the subject of fluid mechanics with double emulsions droplets, is the review of Johnson and Sadhal (1985), and the books of Sadhal *et al.* (1997) and Zapryanov & Tabakova (1999).

Single drops as well as double emulsion droplets in relative viscous fluids are frequently processed in rotating mixing devices experiencing shear or extensional flows. As a result, such drops may translate, deform, rotate or even break, resulting in the modification of the macroscopic properties of the system. The fluid mechanics problem of a single drop undergoing shear or extensional flow has a long history in science, since the pioneering work of Taylor (1932, 1934). While the single drop literature is remarkably extensive with several reviews (Acrivos 1983, 1990; Rallison 1984; Stone 1994; Briscoe, Lawrence & Mietus 1999), much less is the knowledge on the more recent subject of double emulsion droplets. Consider a non-buoyant double emulsion droplet submerged in an external fluid (fluid 1) and subjected to a linear shear or extensional flow. The compound drop is originally composed from a spherical inner drop (fluid 3) enclosed by a spherical fluid shell (fluid 2). We assume all phases to be immiscible, incompressible and Newtonian, and we neglect inertia and gravitational effects. It follows that the fluid mechanics problem, governed by the Stokes equations, is described by several dimensionless numbers. These are: the external capillary number (Ca); two viscosity ratios, shell over external (λ_{21}) and internal over external (λ_{31}); the radii ratio, inner over outer (κ); and the surface tensions ratio, inner-shell over outer-shell (Ω).

Closely related to this work, dealing with shear flow, is a double emulsion droplet in an axisymmetric extensional flow, a case first explored by Stone & Leal (1990). For a stationary concentric spherical double emulsion droplet ($Ca = 0$, $\Omega = \infty$), they showed that when the inner drop is very small ($\kappa \to 0$), the compound drop behaves like a single drop and for a very thin shell ($\kappa \to 1$), the compound drop mimics a solid particle. This interesting and important feature, previously also observed in uniform flow, was recently implemented by Favelukis (2021*a*, 2021*b*) when dealing with external mass transfer problems involving double emulsion droplets. Thus, the external mass transfer rate, which strongly depends on whether the external surface is mobile or immobile, may be adjusted by varying the radii ratio (κ). The small deformation ($Ca \ll 1$) theory of Stone & Leal (1990) suggests that an external uniaxial flow ($Ca > 0$) deforms the outer surface into a prolate spheroid, while the internal drop (which experiences a biaxial flow) deforms into an oblate spheroid. The opposite occurs in an external biaxial flow ($Ca < 0$), meaning an outer oblate spheroid and an inner prolate spheroid. Two types of breakup mechanisms were suggested: in the first one, both surfaces touch each other, while in the second one, the inner drop breaks while leaving the shell continuous. Several extensions to the theoretical treatment of Stone & Leal (1990) have been made; these include the recovery of such a compound drop after the extensional flow is suddenly stopped (Kan *et al.* 1998), an eccentric compound drop in an extensional flow (Qu & Wang 2012; Wang *et al.* 2018), a double emulsion droplet in a nonlinear extensional flow (Favelukis 2020) and a triple emulsion droplet in an extensional flow (Favelukis 2023).

Consider now a double emulsion droplet, but this time, in a simple shear and creeping flow. Davis & Brenner (1981) performed a small-deformation analysis, when the inner phase was a concentric spherical solid. They concluded that a solid inner particle encourages the deformation and breakup of the compound particle. That is, at constant

https://doi.org/10.1017/jfm.2026.11819 Published online by Cambridge University Press

external capillary number (Ca), an increase in the radii ratio (κ) results in a more deformed outer surface. This also leads to a lower critical capillary number in a breakup mechanism were both surfaces touch each other, when compared with a single drop. Chaithanya & Sumesh (2019, 2020) and Singeetham *et al.* (2021) confirmed and extended the findings of Davies & Brenner (1981). It appears that while the $O(Ca^1)$ deformed shape suggests a compound particle oriented along the principal axis of elongation at an angle of 45° with the direction of the flow, the $O(Ca^2)$ deformed shape predicts a smaller angle, similar to the single-drop case. Veerapanneni *et al.* (2011) considered a two-dimensional double emulsion droplet where, as before, the inner phase was a solid particle to mimic a biological cell. Using the boundary integral method, they obtained a numerical solution when the shell and external fluids have the same viscosity. They investigated the rheology as well as the transition of the two main motions of compound vesicles: tank treading and tumbling.

Power (1993) extended the boundary integral method, which is capable to deal numerically with larger deformations of single drops, to the case of double emulsion droplets. A numerical study using a level set approach was conducted by Smith *et al.* (2004). For the case where all phases are of equal densities and viscosities, the compound drop was stretched and then allowed to relax. When shear stops, the drop length decreases and it may break into three or more daughter droplets, which may be single or double. Computational fluid dynamics simulations using the VOF method were performed by Chen, Liu & Shi (2013). For the same external Ca, a double emulsion droplet is less deformed than a single drop. Larger deformations of the inner drop and smaller deformations of the outer surface have been obtained with an increase of the radii ratio (κ). Several breakup mechanisms were also reported: necking, end pinching and capillary instability. The behaviour of a two-dimensional double emulsion droplet was numerically treated by Kravchenko & Patlazhan (2009) and Patlazhan *et al.* (2014) in an unbounded simple shear flow, and by Patlazhan *et al.* (2015) in a confined simple shear flow. The two-dimensional findings are in qualitative agreement with the three-dimensional conclusions described in this section. Another two-dimensional numerical study was conducted by Kaoui *et al.* (2013) to study the behaviour of leukocytes (white blood cells). They found different behaviours of the double emulsion droplet depending on Ca or κ. These include tank-treading, tumbling and undulating motions. They concluded that leukocytes sometimes behave as liquids and sometimes as solids depending on their internal structure and how they are deformed by the external fluid.

A comprehensive numerical study, based on a volume-conserving immersed boundary method, is presented by Hua *et al.* (2014). Although the Reynolds number was not small enough, $Re = O(1)$, we believe their following conclusions can be extrapolated to the creeping flow regime. For the same external Ca, a single drop elongates more than a compound drop. As the radii ratio (κ) increases, the inner drop inclines more towards the flow direction and the outer surface is less elongated. A decrease in the surface tension ratio (Ω) results in a more deformed and inclined internal drop. The angle between the inner drop and the flow direction is always greater or equal to that of the outer surface. An initial eccentric compound drop will eventually, at steady-state, become concentric. Finally, the behaviour difference between simple and double drops increases as the wall becomes more confined. A two-dimensional front-tracking/finite difference numerical method was implemented by Vu *et al.* (2018) to study the transition between steady and breakup of the compound drop in shear flow. Their study, conducted at $Re = O(1)$, $Ca < 1$ and $\Omega = O(1)$, assumes equal densities and viscosities for all phases. Their results were summarised in a phase diagram of Re versus Ca at $\Omega = 1$, showing non-breakup (low Re and Ca) and breakup (high Re and Ca) regions.

https://doi.org/10.1017/jfm.2026.11819 Published online by Cambridge University Press

Mandal *et al.* (2016) explored the effects of insoluble surfactants, being present on both surfaces of the double emulsion droplet, on the small deformation and the effective viscosity in extensional, shear and Poiseuille creeping flows. Similar to this report, they applied Lamb's general solution to the Stokes equations and noted that the presence of surfactants leads to a decrease in the inner drop deformation, yet the outer surface may experience larger or smaller deformations depending on the radii ratio. Surfactants not only introduce a Marangoni stress by varying the surface tension along the surface of the drop, but also induce a surface viscosity. The effects of interfacial shear and dilatational viscosities on the deformation of double emulsion droplets in extensional and shear flows, as well as on the effective viscosity of a dilute emulsion, have been treated by Das *et al.* (2020).

Kim and Dabiri (2017) numerically explored the evolution process of an eccentric compound droplet in a simple shear flow at $Re = O(1)$ and $Ca \ll 1$, using a finite volume and front-tracking methods. In their study, all phases were chosen to have uniform densities and viscosities. When the eccentricity was contained within the plane of shear, the internal drop revolved in that plane while slowly moving outward. However, when the eccentricity was in the direction normal to the plane of shear, the internal drop went a drifting motion slowly moving perpendicular to the plane of shear. Both revolving and drifting motions cause the eccentricity of the double emulsion droplet to increase. Tiribocchi *et al.* (2020) applied lattice Boltzmann simulations to investigate two-dimensional compound drops containing multiple internal drops at $Re = O(1)$. For the case of two internal drops, an oscillatory non-equilibrium steady state is produced where the internal drops periodically rotate around the centre mass of the shell fluid like in a planetary motion.

Apart from the above-mentioned theoretical and numerical reports, several experimental studies on double emulsion droplets in a simple shear flow can be found in the literature. Chen *et al.* (2015*a*) combined experimental and VOF numerical simulations to explore the influence of the inner drop on the double emulsion droplet. As shear starts, the transient behaviour of the double emulsion significantly differs from that of a single drop. While the compound droplet shows a damped oscillation until the deformation is steady, the single drop does not. Also, the time required for the double emulsion to achieve the steady shape is longer than that of the single drop. Finally, they demonstrate that the outer surface of a double emulsion droplet sometimes deforms more and sometimes deforms less, when compared with a single drop. The same group, Chen *et al.* (2015*b*), obtained additional experimental findings regarding the influence of the external capillary number (Ca) and the radii ratio (κ) on the transient and steady behaviour of the double emulsion droplet. It appears that transient damped oscillations increase with an increase in Ca and κ. Also, the angle between the direction of the flow and the largest deformation axis is smaller than 45° for the outer surface and larger than 45° for the inner surface. Furthermore, the outer angle is smaller than that of a single drop (at the same Ca), while the inner angle can be greater than 90°. Finally, the external Taylor deformation parameter was always larger than the internal one, but this may be as a consequence that the rest of the dimensionless parameters (λ_{21}, λ_{31}, Ω) remained constant.

According to Stroeve & Varanasi (1984), the application of double emulsions in separation processes is limited because of the breakup of such drops. Using a cone-and-plate viscometer, they investigated the breakup of double emulsion droplets in shear flow. Similar to single drops, the results can be described by a single plot of the critical external capillary number at breakup (Ca_{cr}) versus the viscosity ratio (λ), defined as the apparent viscosity of the compound droplet to the viscosity of the continuous phase. The plot has the familiar shape to that of a single drop, except that it is shifted to the right to higher values of λ. As the volume of the internal drop increases, equivalent in our case to an

https://doi.org/10.1017/jfm.2026.11819 Published online by Cambridge University Press

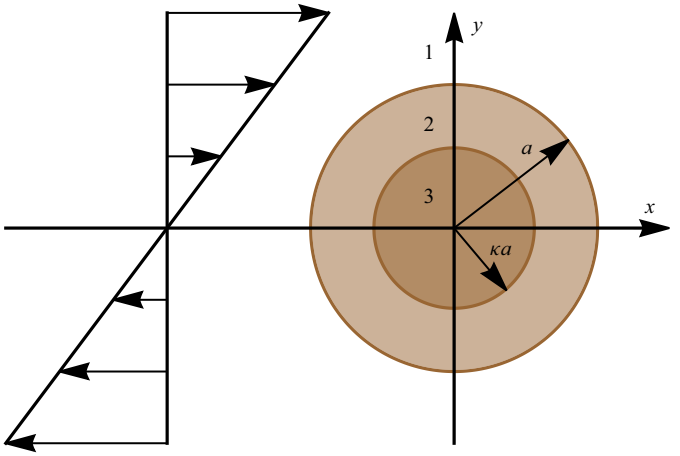


Figure 1. A double emulsion droplet in a simple shear flow ($A > 0$, $C = 0$).

increase in the radii ratio (κ), the plot is shifted more to the right. Thus, if single drops in shear flow cannot be broken at $\lambda > 3.5$, with double emulsion droplets, breakup is not possible at $\lambda > 6$–7.

Levant & Steinberg (2014) reported experimental studies of compound vesicles in linear flows as a model of the behaviour of leukocytes (white blood cells). The experiments were performed in a microfluidic four-roller mill device which can change the flow from rotational to extensional, that is, from closed to open streamlines. This reminds us of the well-known computer four-roll mill apparatus of Bentley & Leal (1986) to study the effect of vorticity on single drops. Levant & Steinberg (2014) concluded that compound vesicles have richer dynamics compared with unilamellar vesicles, but were more difficult to study as a result of the larger number of parameters to be controlled.

Recently, Favelukis (2022) extended the classical papers of Taylor (1932, 1934) and proposed a two-directional nonlinear cubic shear creeping flow. Single-drop deformations in such a nonlinear flow suggest very interesting and unusual shapes, which sometimes are assisted by many stagnation points. Applying Lamb's general solution to the Stokes equations, it was found that for both linear or nonlinear cases, a single drop with $Ca \ll 1$ and $\lambda = O(1)$ is aligned at an azimuth spherical angle $\phi = \pm 45°$. Furthermore, due to the two-directional motion, a spherical drop with no deformation is possible, even when $Ca \neq 0$. In addition, a very viscous drop ($\lambda \gg 1$) remains almost spherical even at $Ca = O(1)$, oriented at $\phi = 0°$ or 90°, with a deformation independent of Ca. It is the purpose of this theoretical communication to go beyond our single-drop two-directional shear findings by obtaining a complete analytical solution of $O(Ca^0)$, as well as to examine small deformations at $O(Ca^1)$, of a double emulsion droplet in a two-directional linear shear flow under creeping flow conditions.

2. Governing equations

Figure 1 describes a stationary non-buoyant double emulsion droplet positioned at the origin of a Cartesian coordinate system (x, y, z). The double emulsion droplet is made from an inner spherical drop of radius κa (fluid 3), completely embedded by a spherical fluid shell having an external radius a (fluid 2). Far away, the external fluid (fluid 1) is subjected to a two-directional shear flow, defined as

https://doi.org/10.1017/jfm.2026.11819 Published online by Cambridge University Press

$$v_x = Ay, \tag{2.1}$$

$$v_y = Cx, \tag{2.2}$$

$$v_z = 0, \tag{2.3}$$

$$p = K, \tag{2.4}$$

where p is the pressure and K is a constant. We allow the constants A and C to be positive or negative, and when $C = 0$ and $A > 0$, the familiar simple shear flow in the x direction is recovered, as illustrated in figure 1.

The undisturbed motion, given by (2.1)–(2.4), can be written in spherical coordinates (r, θ, ϕ), with $0 \leq \theta \leq \pi$ being the polar angle and $0 \leq \phi < 2\pi$ the azimuth angle, as follows:

$$v_r = \frac{1}{2}(A + C)\, r \sin^2\theta \sin(2\phi), \tag{2.5}$$

$$v_\theta = \frac{1}{2}(A + C)\, r \cos\theta \sin\theta \sin(2\phi), \tag{2.6}$$

$$v_\phi = \frac{1}{2} r \sin\theta\, [-A + C + (A + C)\cos(2\phi)], \tag{2.7}$$

$$p = K. \tag{2.8}$$

Taking the dimensionless form of the Stokes equations in all three phases, as well as the boundary conditions described later, one finds out that this physical situation is governed by six dimensionless numbers. These are: the external capillary number (Ca); two viscosity ratios, shell over external (λ_{21}), and internal over external (λ_{31}); the radii ratio, internal over external (κ); the surface tensions ratio, internal-shell over external-shell (Ω); and the flow-type parameter (G):

$$Ca = \frac{\mu_1 A a}{\sigma}, \tag{2.9}$$

$$\lambda_{21} = \frac{\mu_2}{\mu_1}, \tag{2.10}$$

$$\lambda_{31} = \frac{\mu_3}{\mu_1}, \tag{2.11}$$

$$\kappa = \frac{\kappa a}{a}, \tag{2.12}$$

$$\Omega = \frac{\sigma_{32}}{\sigma_{21}}, \tag{2.13}$$

$$G = \frac{C}{A}. \tag{2.14}$$

Here, μ is the viscosity, a is the outer radius and σ is the surface tension. The subscripts 1, 2 and 3 denote the different phases according to figure 1, and the subscripts 21 and 32 represent the outer and inner interfaces, respectively. Since the constants A and C can be positive, negative or zero, the same can be said for Ca and G.

Let the lengths be rendered dimensionless with respect to the outer radius (a), the velocities with a characteristic velocity ($U = Aa$), and the pressures (p) and viscous stresses (τ) with the characteristic external stress ($\mu_1 A$). Based on Lamb's general solution to the Stokes equations in spherical coordinates (Lamb 1945; Happel & Brenner 1983;

https://doi.org/10.1017/jfm.2026.11819 Published online by Cambridge University Press

Zapryanov & Tabakova 1999), we can construct a solution procedure to this problem by following the guidelines of Mandal *et al.* (2016).

For the external fluid (fluid 1), the velocity is composed from the undisturbed motion ($\boldsymbol{v}_\infty$) plus the disturbance, which is composed from decaying harmonics together with the usual substitution by replacing n with $-(n+1)$:

$$\boldsymbol{v}_1 = \boldsymbol{v}_\infty + \sum_{n=1}^{\infty}\left[-\frac{(n-2)r^2\nabla p1_{-n-1}}{2n(2n-1)} + \frac{(n+1)\,r\boldsymbol{e}_r p1_{-n-1}}{n(2n-1)} + \nabla\Phi 1_{-n-1}\right.$$
$$\left.+\nabla\times(r\boldsymbol{e}_r\chi 1_{-n-1})\right], \tag{2.15}$$

$$p_1 = p_\infty + \sum_{n=1}^{\infty} p1_{-n-1}, \tag{2.16}$$

$$p1_{-n-1} = r^{-n-1}\sum_{m=0}^{n} P_n^m(\eta)\left[a1_{-n-1,m}\cos(m\phi) + b1_{-n-1,m}\sin(m\phi)\right], \tag{2.17}$$

$$\Phi 1_{-n-1} = r^{-n-1}\sum_{m=0}^{n} P_n^m(\eta)\left[c1_{-n-1,m}\cos(m\phi) + d1_{-n-1,m}\sin(m\phi)\right], \tag{2.18}$$

$$\chi 1_{-n-1} = r^{-n-1}\sum_{m=0}^{n} P_n^m(\eta)\left[e1_{-n-1,m}\cos(m\phi) + f1_{-n-1,m}\sin(m\phi)\right]. \tag{2.19}$$

For the shell fluid (fluid 2), the velocity must be composed from both decaying and growing harmonics:

$$\boldsymbol{v}_2 = \sum_{n=1}^{\infty}\left[-\frac{(n-2)r^2\nabla p2_{-n-1}}{2\lambda_{21}n(2n-1)} + \frac{(n+1)\,r\boldsymbol{e}_r p2_{-n-1}}{\lambda_{21}n(2n-1)} + \nabla\Phi 2_{-n-1}\right.$$
$$\left.+\nabla\times(r\boldsymbol{e}_r\chi 2_{-n-1})\right] + \sum_{n=1}^{\infty}\left[\frac{(n+3)\,r^2\nabla p2_n}{2\lambda_{21}\,(n+1)\,(2n+3)} - \frac{nr\boldsymbol{e}_r p2_n}{\lambda_{21}\,(n+1)\,(2n+3)}\right.$$
$$\left.+\nabla\Phi 2_n + \nabla\times(r\boldsymbol{e}_r\chi 2_n)\right], \tag{2.20}$$

$$p_2 = p_{shell} + \sum_{n=1}^{\infty} p2_{-n-1} + \sum_{n=1}^{\infty} p2_n, \tag{2.21}$$

$$p2_{-n-1} = r^{-n-1}\sum_{m=0}^{n} P_n^m(\eta)\left[a2_{-n-1,m}\cos(m\phi) + b2_{-n-1,m}\sin(m\phi)\right], \tag{2.22}$$

$$\Phi 2_{-n-1} = r^{-n-1}\sum_{m=0}^{n} P_n^m(\eta)\left[c2_{-n-1,m}\cos(m\phi) + d2_{-n-1,m}\sin(m\phi)\right], \tag{2.23}$$

$$\chi 2_{-n-1} = r^{-n-1}\sum_{m=0}^{n} P_n^m(\eta)\left[e2_{-n-1,m}\cos(m\phi) + f2_{-n-1,m}\sin(m\phi)\right], \tag{2.24}$$

$$p2_n = r^{n}\sum_{m=0}^{n} P_n^m(\eta)\left[a2_{n,m}\cos(m\phi) + b2_{n,m}\sin(m\phi)\right], \tag{2.25}$$

https://doi.org/10.1017/jfm.2026.11819 Published online by Cambridge University Press

$$\Phi 2_n = r^n \sum_{m=0}^{n} P_n^m(\eta)\left[c2_{n,m}\cos(m\phi) + d2_{n,m}\sin(m\phi)\right], \tag{2.26}$$

$$\chi 2_n = r^n \sum_{m=0}^{n} P_n^m(\eta)\left[e2_{n,m}\cos(m\phi) + f2_{n,m}\sin(m\phi)\right]. \tag{2.27}$$

Finally, only growing harmonics are necessary for the internal drop (fluid 3):

$$\boldsymbol{v}_3 = \sum_{n=1}^{\infty}\left[\frac{(n+3)\,r^2\nabla p3_n}{2\lambda_{31}\,(n+1)\,(2n+3)} - \frac{nr\boldsymbol{e}_r p3_n}{\lambda_{31}\,(n+1)\,(2n+3)} + \nabla\Phi 3_n + \nabla\times(r\boldsymbol{e}_r\chi 3_n)\right], \tag{2.28}$$

$$p_3 = p_0 + \sum_{n=1}^{\infty} p3_n, \tag{2.29}$$

$$p3_n = r^n \sum_{m=0}^{n} P_n^m(\eta)\left[a3_{n,m}\cos(m\phi) + b3_{n,m}\sin(m\phi)\right], \tag{2.30}$$

$$\Phi 3_n = r^n \sum_{m=0}^{n} P_n^m(\eta)\left[c3_{n,m}\cos(m\phi) + d3_{n,m}\sin(m\phi)\right], \tag{2.31}$$

$$\chi 3_n = r^n \sum_{m=0}^{n} P_n^m(\eta)\left[e3_{n,m}\cos(m\phi) + f3_{n,m}\sin(m\phi)\right]. \tag{2.32}$$

Here, $\boldsymbol{v}$ is the velocity vector, $\boldsymbol{v}_\infty$ and p_∞ are the velocity vector and pressure of the undisturbed motion, p_{shell} and p_0 are the shell and inner drop pressures in the absence of flow, respectively, and $\boldsymbol{e}_r$ is the unit vector in the radial direction. The functions p_n, Φ_n and χ_n (and also those with the subscript $-n-1$) are solid spherical harmonics, $P_n{}^m(\eta)$ is the associated Legendre polynomial of degree n and order m, and, as usual, $\eta = \cos\theta$. The large amount of constants appearing in (2.15)–(2.32), will be evaluated according to the usual boundary conditions.

According to the no-slip condition, equal normal velocities are required at each interface. Furthermore, in a stationary double emulsion droplet, all normal velocities vanish:

$$\text{at } r = 1:\ v_{1,r} = v_{2,r} = 0, \tag{2.33}$$

$$\text{at } r = \kappa:\ v_{2,r} = v_{3,r} = 0, \tag{2.34}$$

$$\text{at } r = 1:\ v_{1,\theta} = v_{2,\theta}, \tag{2.35}$$

$$\text{at } r = \kappa:\ v_{2,\theta} = v_{3,\theta}, \tag{2.36}$$

$$\text{at } r = 1:\ v_{1,\phi} = v_{2,\phi}, \tag{2.37}$$

$$\text{at } r = \kappa:\ v_{2,\phi} = v_{3,\phi}. \tag{2.38}$$

According to Newton's third law of motion, the normal and tangential stresses must be balanced at each interface. The tangential stress suggests

$$\text{at } r = 1:\ \tau_{1,r\theta} = \tau_{2,r\theta}, \tag{2.39}$$

$$\text{at } r = \kappa:\ \tau_{2,r\theta} = \tau_{3,r\theta}, \tag{2.40}$$

$$\text{at } r = 1:\ \tau_{1,r\phi} = \tau_{2,r\phi}, \tag{2.41}$$

$$\text{at } r = \kappa:\ \tau_{2,r\phi} = \tau_{3,r\phi}. \tag{2.42}$$

https://doi.org/10.1017/jfm.2026.11819 Published online by Cambridge University Press

Equations (2.15)–(2.42) complete the requirements for the spherical solution ($Ca = 0$). Upon substituting this $O(Ca^0)$ solution into the normal stress balance, the $O(Ca^1)$ deformed shape can be obtained:

$$\text{at } r = 1: \; p_2 - p_1 + \tau_{1,rr} - \tau_{2,rr} = \frac{1}{Ca}\left(\frac{1}{R_{21,\alpha}} + \frac{1}{R_{21,\beta}}\right), \tag{2.43}$$

$$\text{at } r = \kappa: \; p_3 - p_2 + \tau_{2,rr} - \tau_{3,rr} = \frac{\Omega}{Ca}\left(\frac{1}{R_{32,\alpha}} + \frac{1}{R_{32,\beta}}\right), \tag{2.44}$$

where $R_{ij,\alpha}$ and $R_{ij,\beta}$ are the principal radii of curvature at each interface. For the outer interface, $ij = 21$ and for the inner one, $ij = 32$.

3. Undisturbed motion

Before exploring the motion of a double emulsion droplet in a two-directional shear flow, it will be beneficial to inspect first the flow in the absence of the drop. For this incompressible two-dimensional motion, a stream function can be easily obtained:

$$v_x = +\frac{\partial \psi}{\partial y} = y, \tag{3.1}$$

$$v_y = -\frac{\partial \psi}{\partial x} = Gx, \tag{3.2}$$

$$\psi = \frac{1}{2}\left(y^2 - Gx^2\right). \tag{3.3}$$

Note that v_x and v_y vanish only at the origin.

The only non-vanishing terms of the strain rate tensor (Γ) and of the vorticity tensor (Ω) are

$$\Gamma_{xy} = \Gamma_{yx} = \frac{1}{2}\left(1 + G\right), \tag{3.4}$$

$$\Omega_{xy} = -\Omega_{yx} = \frac{1}{2}\left(G - 1\right). \tag{3.5}$$

Consider the flow-type parameter G. When $G = 0$, the familiar simple shear flow in the x-direction only, having angular deformation and rotation of the same magnitude, is recovered. Also, when $G = 1$, there is only angular deformation and if $G = -1$, there is rotation only.

A velocity vector plot of the undisturbed motion is described in figure 2. Four cases are illustrated. The first two describe the familiar simple shear flow in the x-direction ($G = 0$) and in the y-direction ($G = \infty$). The third one represents angular deformation without rotation ($G = 1$) or an extensional flow from a $\phi = \pm 45°$ point of view. Finally, the fourth case ($G = -1$) depicts a clockwise rotation without angular deformation. Now that we are familiar with the undisturbed motion, we can introduce a double emulsion droplet in such a flow and explore its behaviour.

4. Disturbed motion

The disturbed motion, that is, the flow in the presence of the double emulsion droplet, is discussed in this section. We assume here all interfaces to be spherical, corresponding to the asymptotic limit of $Ca = 0$ and $\Omega = \infty$. For this case, the problem is governed by four dimensionless parameters only: λ_{21}, λ_{31}, κ and G. The solution is obtained by

https://doi.org/10.1017/jfm.2026.11819 Published online by Cambridge University Press

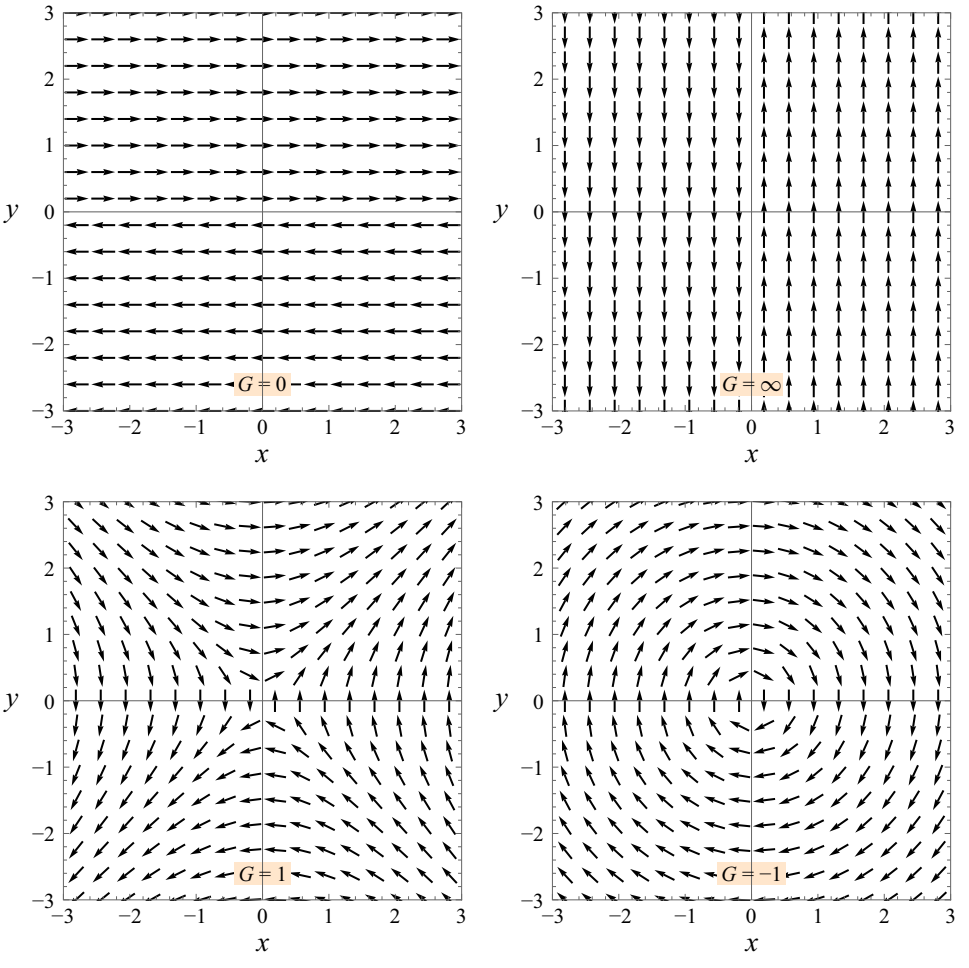


Figure 2. The undisturbed motion.

substituting the boundary conditions, given by (2.33)–(2.42), into Lamb's general solution to the Stokes equations in spherical coordinates, expressed by (2.15)–(2.32). With the assistance of the Mathematica software and after a long algebraic manipulation, the following analytical expressions for the coefficients of the solid harmonics were obtained. For the external fluid (fluid 1), we have coefficients with $n = 2$ only:

$$b1_{-3,2} = -\frac{(1+G)}{3}\left[\frac{10H_1\lambda_{21}{}^2 + (1-\kappa)^2\, H_2\lambda_{31} + H_3\lambda_{21}\,(2+5\lambda_{31})}{4H_1\lambda_{21}{}^2 + (1-\kappa)^2\, H_2\lambda_{31} + 2H_3\lambda_{21}\,(1+\lambda_{31})}\right], \tag{4.1}$$

$$d1_{-3,2} = -\frac{(1+G)\,\lambda_{21}}{6}\left[\frac{2H_1\lambda_{21} + H_3\lambda_{31}}{4H_1\lambda_{21}{}^2 + (1-\kappa)^2\, H_2\lambda_{31} + 2H_3\lambda_{21}\,(1+\lambda_{31})}\right]. \tag{4.2}$$

The coefficients of the shell (fluid 2) include $n = 1$ and $n = 2$:

$$b2_{-3,2} = +\frac{(1+G)\,\kappa^3\lambda_{21}}{(1-\kappa)}\left[\frac{2H_4\lambda_{21} + H_5\lambda_{31}}{4H_1\lambda_{21}{}^2 + (1-\kappa)^2\, H_2\lambda_{31} + 2H_3\lambda_{21}\,(1+\lambda_{31})}\right], \tag{4.3}$$

https://doi.org/10.1017/jfm.2026.11819 Published online by Cambridge University Press

$$d2_{-3,2} = +\frac{(1+G)\,\kappa^5}{6\,(1-\kappa)}\left[\frac{2\kappa^2 H_6\,(\lambda_{21}-\lambda_{31})+3\,(1+\kappa)\,\lambda_{31}}{4H_1{\lambda_{21}}^2+(1-\kappa)^2\,H_2\lambda_{31}+2H_3\lambda_{21}\,(1+\lambda_{31})}\right], \tag{4.4}$$

$$b2_{2,2} = +\frac{7\,(1+G)\,\lambda_{21}}{2\,(1-\kappa)}\left[\frac{2H_6\lambda_{21}+H_7\lambda_{31}}{4H_1{\lambda_{21}}^2+(1-\kappa)^2\,H_2\lambda_{31}+2H_3\lambda_{21}\,(1+\lambda_{31})}\right], \tag{4.5}$$

$$d2_{2,2} = -\frac{(1+G)}{4\,(1-\kappa)}\left[\frac{2H_4\lambda_{21}+H_8\lambda_{31}}{4H_1{\lambda_{21}}^2+(1-\kappa)^2\,H_2\lambda_{31}+2H_3\lambda_{21}\,(1+\lambda_{31})}\right], \tag{4.6}$$

$$e2_{1,0} = -\frac{(1-G)}{2}. \tag{4.7}$$

Finally, the inner drop (fluid 3) coefficients consist of $n=1$ and $n=2$:

$$b3_{2,2} = -\frac{7\,(1+G)\,(1-\kappa)\,\lambda_{21}\lambda_{31}}{2\kappa^2}\left[\frac{H_9}{4H_1{\lambda_{21}}^2+(1-\kappa)^2\,H_2\lambda_{31}+2H_3\lambda_{21}\,(1+\lambda_{31})}\right], \tag{4.8}$$

$$d3_{2,2} = +\frac{(1+G)\,(1-\kappa)\,\lambda_{21}}{4}\left[\frac{H_9}{4H_1{\lambda_{21}}^2+(1-\kappa)^2\,H_2\lambda_{31}+2H_3\lambda_{21}\,(1+\lambda_{31})}\right], \tag{4.9}$$

$$e3_{1,0} = -\frac{(1-G)}{2}, \tag{4.10}$$

where the rest of the coefficients vanish. Inside the square brackets, H_i with $i=1$–9 are functions of the radii ratio (κ) only and are listed in the Appendix A.

Figure 3 explores the disturbed motion, in the xy plane ($z=\eta=0$), of a double emulsion droplet with $\lambda_{31}=1$ and $\kappa=1/2$ for the familiar simple shear flow ($G=0$) in the x-direction only. Four different shell fluid to external fluid viscosity ratios (λ_{21}) are presented, ranging from an inviscid shell ($\lambda_{21}=0$) up to a solid shell ($\lambda_{21}=\infty$). Note that when $z=0$, the z-velocity component in all phases vanishes, resulting in a two-dimensional motion and, therefore, a streamline discussion in the xy plane is permitted. The first case, corresponding to an inviscid shell ($\lambda_{21}=0$), is the only one with open external streamlines. The shell fluid suggests oval streamlines, while the streamlines of the inner drop fluid are exact circles. Here, the inner drop fluid rotates at an angular velocity of $\omega=-(1-G)/2$ regardless the values of λ_{31} and κ. The next two cases ($\lambda_{21}=0.1$, $\lambda_{21}=1$) suggest that as λ_{21} increases, the shell fluid becomes less oval, but the inner drop fluid becomes oval. Note that the major axis of the shell oval is perpendicular to the major axis of the inner drop oval. Finally, for a solid shell ($\lambda_{21}=\infty$), the streamlines of the shell and of the inner drop fluids are completely circular, with both phases rotating once again at an angular velocity of $\omega=-(1-G)/2$ independently of λ_{31} and κ. Apart from the origin, no stagnation points have been detected, except of the inviscid shell ($\lambda_{21}=0$), where external surface ($r=1$) stagnation points are located at $\phi=0^\circ$ and $\phi=180^\circ$, necessarily to create external open streamlines.

In figure 4, we investigate the influence of the inner drop to external fluid viscosity ratio (λ_{31}) on a double emulsion droplet with $\lambda_{21}=1$ and $\kappa=1/2$, in a simple shear flow ($G=0$). All four λ_{31} cases suggest external closed streamlines and slightly oval streamlines in the shell fluid. The main difference between the different cases appears to be in the inner drop. As λ_{31} increases, the internal streamlines become less oval, until the case of an internal solid sphere ($\lambda_{31}=\infty$), where the streamlines are circles. Here, the solid inner sphere rotates at $\omega=-(1-G)/2$ regardless the values of λ_{21} and κ. Apart from the origin, no stagnation points are present in figure 4.

https://doi.org/10.1017/jfm.2026.11819 Published online by Cambridge University Press

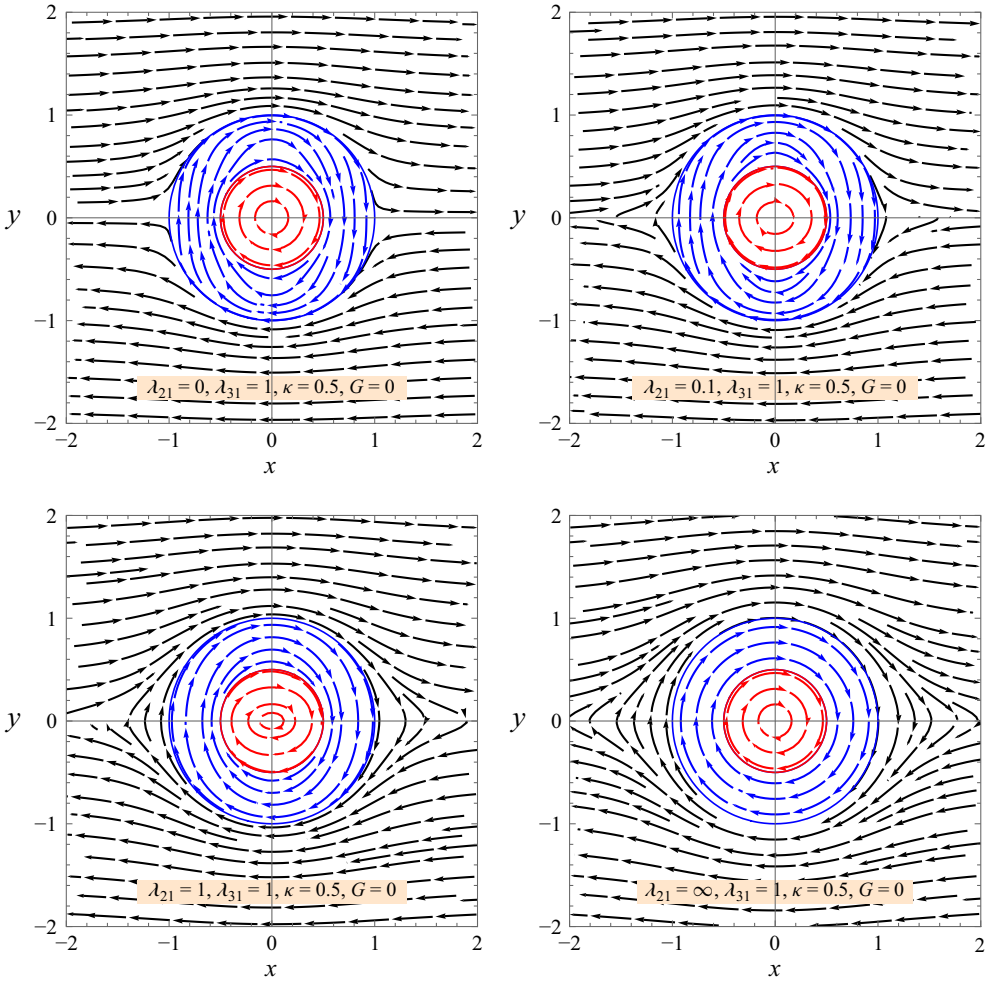


Figure 3. The disturbed motion with $\lambda_{31} = 1$, $\kappa = 1/2$ and $G = 0$, as a function of λ_{21}.

Next, in figure 5, we describe the influence of the radii ratio (κ) on a double emulsion droplet with $\lambda_{21} = 1$ and $\lambda_{31} = 1$ in a simple shear flow ($G = 0$). From our past observations in figure 3, we reconfirm that since $\lambda_{21} \neq 0$, all external streamlines are closed. As κ increases, both the shell fluid and the inner drop fluid become less oval. In the limit of $\kappa \to 1$, the thickness of the shell is infinitely small, and both shell and inner drop behave like solids rotating at an angular velocity of $\omega = -(1 - G)/2$ regardless the values of λ_{21} and λ_{31}. Once again, apart from the origin, no stagnation points are present in figure 5.

At this point, it is interesting to compare the asymptotic limit of $\kappa \to 1$, between simple shear flow ($G = 0$) and simple extensional flow or uniform flow (Stone & Leal 1990; Favelukis 2020; Favelukis 2021*a*; Favelukis 2021*b*). In simple shear, the shell fluid flows in one direction only, whereas in an extensional flow or in uniform flow, the shell fluid near the external fluid flows in the opposite direction to the shell fluid near the inner drop. This change in flow directions of the shell fluid over a very short distance results in a zero tangential velocity, as in a solid boundary.

So far, our discussion has been focused on simple shear flow ($G = 0$) and we noticed that, apart from the origin, no stagnation points have been located, except when the shell is

https://doi.org/10.1017/jfm.2026.11819 Published online by Cambridge University Press

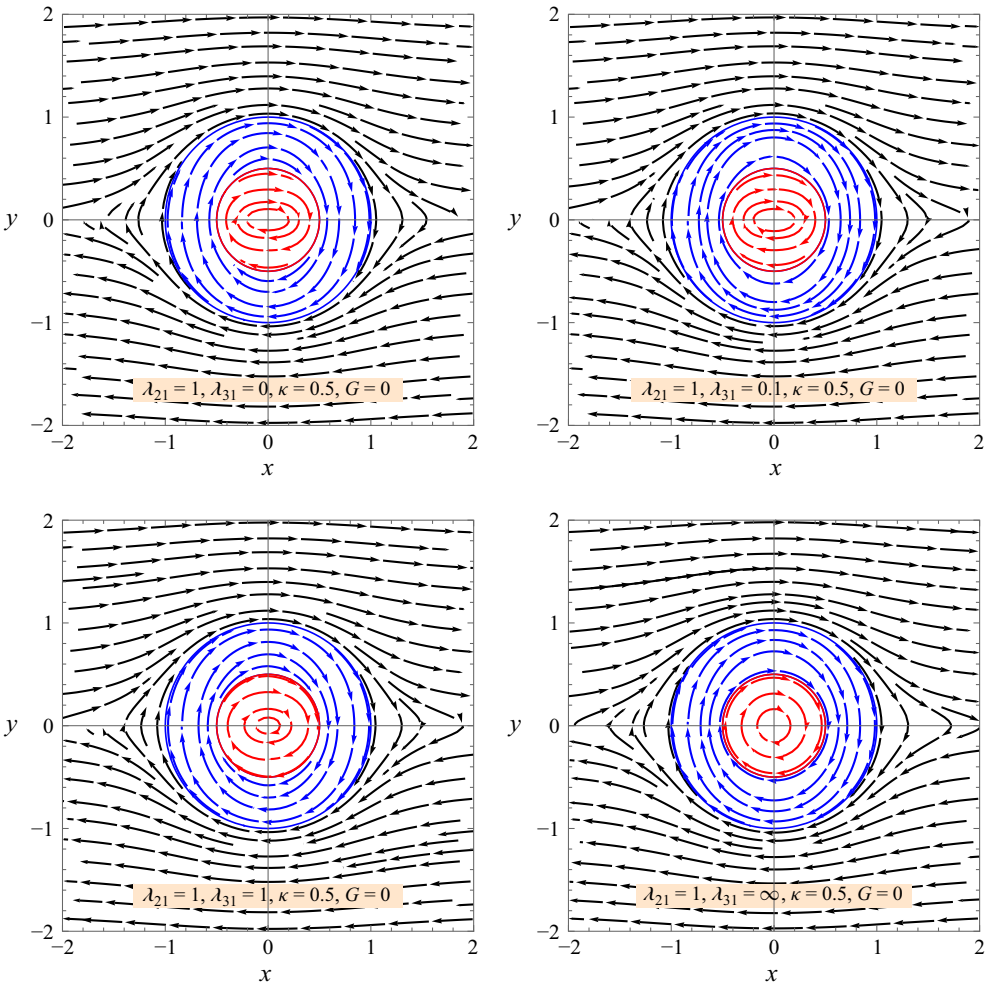


Figure 4. The disturbed motion with $\lambda_{21} = 1$, $\kappa = 1/2$ and $G = 0$, as a function of λ_{31}.

inviscid ($\lambda_{21} = 0$) and the external streamlines are open. These surface stagnations points, in the xy plane, are found to be at the surface of the drop ($r = 1$) at $\phi = 0°$ and $\phi = 180°$. For a single drop in a simple shear flow, with λ being the viscosity ratio (drop to external fluid), Bartok & Mason (1958) found out that when $\lambda < 1/2$, the internal streamlines suggest an 8 shape with two additional stagnation points inside the drop at $\phi = 90°$ and $\phi = 270°$ and at $r = \sqrt{(1 - 2\lambda)/5}$.

Stagnation points, in a double emulsion droplet with $\lambda_{21} = 0$ and $\lambda_{31} = 1$ in a simple shear flow ($G = 0$), are presented in figure 6 by the solid purple circles. The first case corresponds to an inviscid single drop ($\lambda = 0$, $\kappa = 0$), where the two stagnation points, apart from those the origin and at the surface, are located at $\phi = 90°$ and $\phi = 270°$ and at $r = \sqrt{1/5} = 0.447$. In contrast to the single drop, and apart from the origin and the external surface, the double emulsion droplet may contain, at $\phi = 90°$ and $\phi = 270°$, up to four stagnation points in the shell fluid, see table 1. The cases $\kappa = 0.1$ and $\kappa = 0.2$ contain four stagnation points. As κ continues to increase, these points move towards each other until they become one, at the limit of $\kappa = 0.294$. Beyond this limit, no stagnation points, at $\phi = 90°$ and $\phi = 270°$, are located. It is interesting to note that for $\lambda_{21} = 0$, the stagnation

https://doi.org/10.1017/jfm.2026.11819 Published online by Cambridge University Press

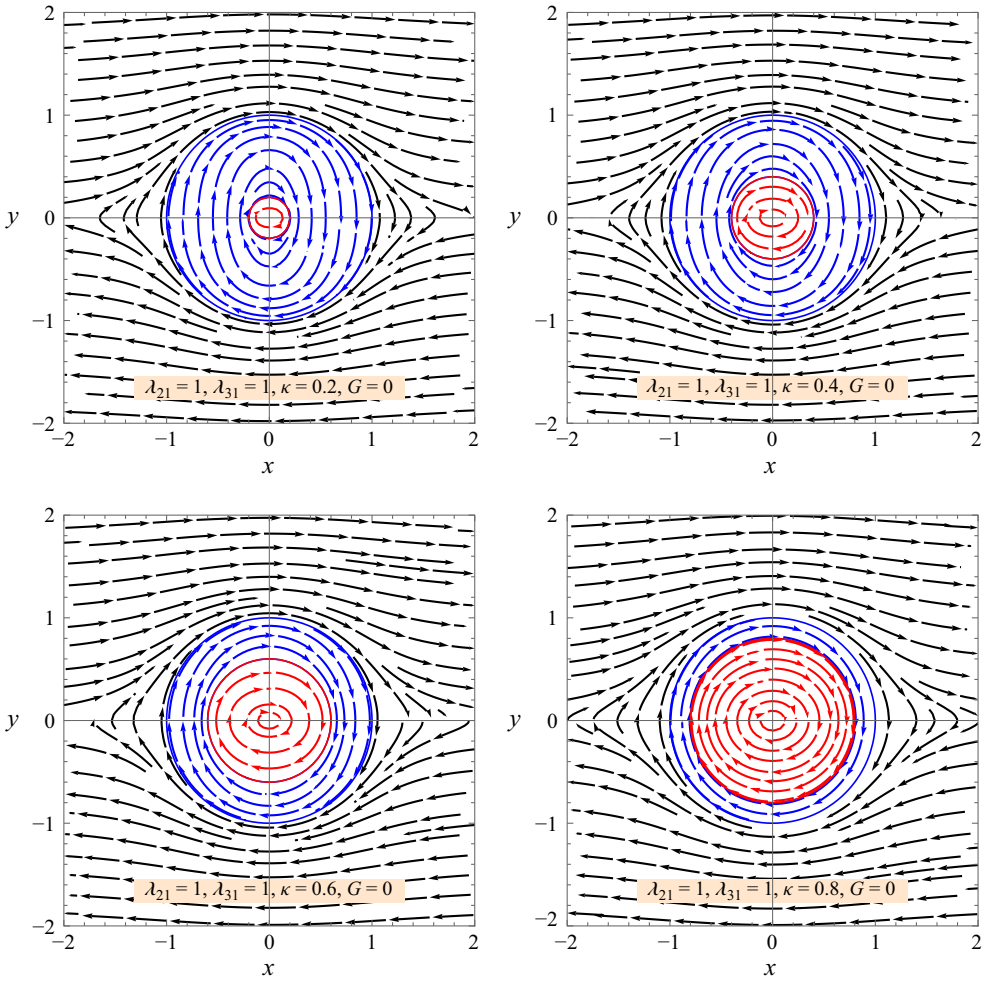


Figure 5. The disturbed motion with $\lambda_{21} = 1$, $\lambda_{31} = 1$ and $G = 0$, as a function of κ.

values in table 1 are independent of λ_{31}. Yet, this is not the case if $\lambda_{21} \neq 0$, where these points will depend on λ_{31}. No shell stagnation points at $\phi = 90°$ and $\phi = 270°$ have been detected if $\lambda_{21} > 1/2$ regardless the values of λ_{31} or κ.

The influence of the flow-type parameter (G) on a double emulsion droplet with $\lambda_{21} = 1$, $\lambda_{31} = 1$ and $\kappa = 1/2$ is described in figure 7. The upper panels show positive G values, while the lower ones represent negative values of G. In the first case ($G = 1$), and from a $\phi = \pm 45°$ point of view, the undisturbed motion represents an extensional flow. Here, both the shell and the inner drop are divided into four sections, with each section containing a closed circulation. This structure requires many stagnation points in the shell and the inner drop fluids, as well as in the inner and outer surfaces of the double emulsion droplet. In the next case ($G = 3$), the external fluid velocity in the y-direction is much larger than that in the x-direction. The streamlines in the shell and in the inner drop are oval but are tilted at $\phi = \pm 90°$ when compared with the streamlines in figures 3–6, for the case of simple shear flow. Another difference between this case ($G = 3$) and simple shear flow ($G = 0$) is that, here, the external streamlines are open, while in simple shear flow (except for $\lambda_{21} = 0$), they are closed. The first negative flow-type parameter ($G = -1$) case suggests clockwise

https://doi.org/10.1017/jfm.2026.11819 Published online by Cambridge University Press

λ_{21}	κ	r
0	0	0.447
0	0.1	0.126, 0.450
0	0.2	0.260, 0.462
0	0.294	0.436

Table 1. Stagnation points at $\phi = 90°$ and $\phi = 270°$ for a double emulsion droplet with $\lambda_{21} = 0$ and $G = 0$, as a function of κ.

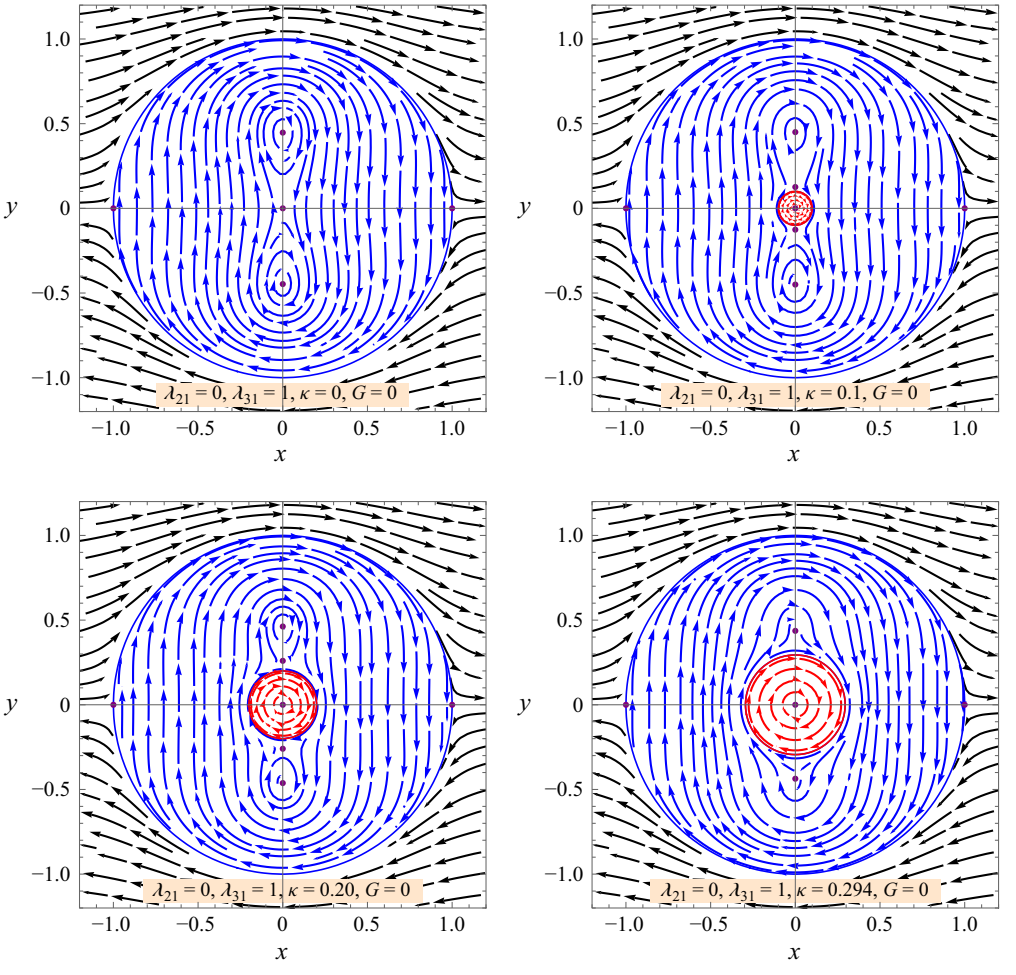


Figure 6. Stagnation points in the disturbed motion with $\lambda_{21} = 0$, $\lambda_{31} = 1$ and $G = 0$, as a function of κ.

rotation with an angular velocity $\omega = -1$ in all three fluids regardless the values of λ_{21}, λ_{31} or κ. Thus, the presence of the double emulsion droplet does not alter the undisturbed motion, which is the same as the disturbed flow. As the flow-type parameter becomes more negative ($G = -3$), the streamlines change their configuration from circles towards oval shapes, most notably in the external fluid.

https://doi.org/10.1017/jfm.2026.11819 Published online by Cambridge University Press

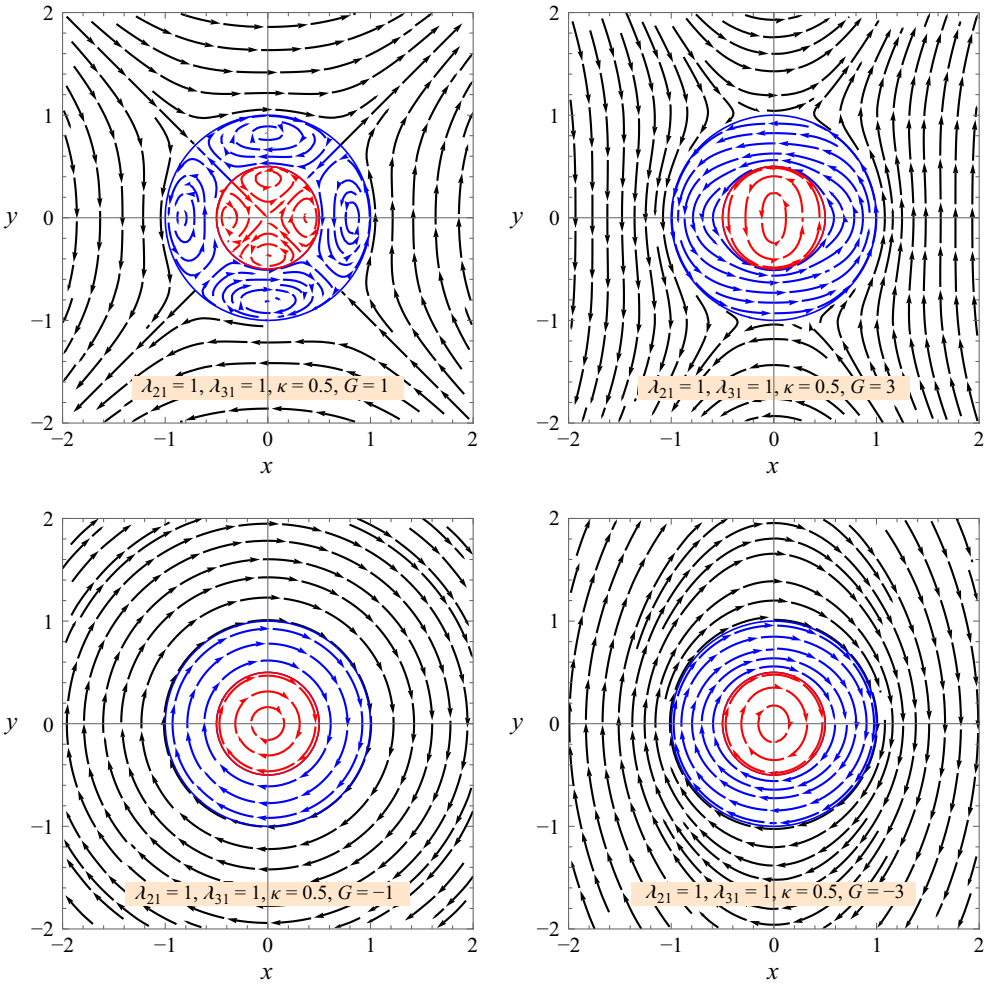


Figure 7. The disturbed motion with $\lambda_{21} = 1$, $\lambda_{31} = 1$ and $\kappa = 1/2$, as a function of G.

5. Deformation of a double emulsion droplet

At present, we have the velocity and stress profile inside and outside a spherical double emulsion droplet, corresponding to the asymptotic limit of $Ca = 0$ and $\Omega = \infty$ and, thus, representing the $O(Ca^0)$ solution. This was obtained by solving the Stokes equations with the appropriate boundary conditions, except of the normal stress balance, which will be applied now to find the $O(Ca^1)$ deformed shape.

Let us define the distance from the origin to the outer surface (21) and to the inner surface (32) of the double emulsion droplet as follows:

$$R_{21}(\eta, \phi) = 1 + Ca f_{21}(\eta, \phi), \tag{5.1}$$

$$R_{32}(\eta, \phi) = \kappa \left[1 + Ca f_{32}(\eta, \phi)\right]. \tag{5.2}$$

Following Landau & Lifshitz (1987), the shapes functions f_{21} and f_{32} are related to the principal radii of curvature in the following way:

https://doi.org/10.1017/jfm.2026.11819 Published online by Cambridge University Press

$$\frac{1}{R_{21,\alpha}}+\frac{1}{R_{21,\beta}}=2-Ca\left(2f_{21}+\nabla^2 f_{21}\right), \tag{5.3}$$

$$\frac{1}{R_{32,\alpha}}+\frac{1}{R_{32,\beta}}=\frac{1}{\kappa}\left[2-Ca\left(2f_{32}+\nabla^2 f_{32}\right)\right]. \tag{5.4}$$

The $O(Ca^0)$ solution can be substituted into the normal stress balances, given by (2.43) and (2.44), to find the principal radii of curvature at each interface. Combining this last result with (5.3) and (5.4), and after some algebraic manipulation, analytical expressions (long and cumbersome) for the two surfaces of the deformed double emulsion droplet can be obtained. An elegant and compact way to present the shape is to perform a Taylor series for the radii ratio (κ) around $\kappa=0$. The leading terms take the form of

$$R_{21}=1+Ca\,(1+G)\left(1-\eta^2\right)\sin(2\phi)\left[\frac{(16+19\lambda_{21})}{(16+16\lambda_{21})}\right.$$
$$\left.+\frac{3\lambda_{21}\,(19+16\lambda_{21})\,(2\lambda_{21}+5\lambda_{31})}{64\,(1+\lambda_{21})^2\,(\lambda_{21}+\lambda_{31})}\kappa^3\right]. \tag{5.5}$$

$$R_{32}=\kappa\left[1-\frac{Ca}{\Omega}\,(1+G)\left(1-\eta^2\right)\sin(2\phi)\frac{\lambda_{21}\,(16\lambda_{21}+19\lambda_{31})}{(16+16\lambda_{21})\,(\lambda_{21}+\lambda_{31})}\kappa^3\right]. \tag{5.6}$$

When $\kappa=0$, the inner drop disappears ($R_{32}=0$), the double emulsion becomes a single drop and (5.5) reduces to the familiar expression presented in the literature with the viscosity ratio λ (drop to external fluid) replacing λ_{21}. The largest and smallest axes of the deformed shapes in the xy ($\eta=0$) plane can be found by letting $\partial R_{21}/\partial\phi=0$ or $\partial R_{32}/\partial\phi=0$. Clearly, these are located at the principal axes of extension or compression ($\phi=\pm45°$). The solution presented here is valid for a slightly deformed double emulsion droplet and, therefore, the following conditions must apply: $\lambda_{21}=O(1)$, $\lambda_{32}=O(1)$, $G=O(1)$, $Ca\ll1$ and $Ca/\Omega\ll1$.

Figure 8 describes the deformation of a double emulsion droplet with $\lambda_{21}=1$, $\lambda_{31}=1$, $\kappa=1/2$, $G=0$ (simple shear flow) and $\Omega=1$, as a function of Ca. Figure 8, and the deformation figures that follow, show the exact $O(Ca^1)$ solution and not the approximations in (5.5) and (5.6). In all cases of figure 8, the outer surface (R_{21}) is more deformed than the inner surface (R_{32}). The major axis of R_{21} is at $\phi=+45°$, while the major axis of R_{32} is at $\phi=-45°$, so they are orthogonal. As the capillary number (Ca) increases, the deformation of both surfaces increases, the outer surface attains a peanut shape, until both surfaces touch each other at a critical value of $Ca=15\,653/40\,915=0.383$. We shall call this critical point as the $R_{21}=R_{32}$ breakup mechanism. It is understood that this is not the official breakup point since the breakup mechanism is a complicated transient unstable situation in which the steady and $O(Ca^1)$ deformed shape cannot predict. Yet, we feel that this is a valuable information to the reader. Note that, at $\phi=0°$, 90°, 180° and 270°, $R_{21}=1$ and $R_{32}=\kappa$, as can be easily confirmed by (5.5) and (5.6).

Next, in figure 9, is the influence of Ca on the deformation of the same double emulsion droplet as in figure 8 ($\lambda_{21}=1$, $\lambda_{31}=1$, $\kappa=1/2$, $\Omega=1$), except that this time, instead of simple shear flow ($G=0$), we have $G=1$. Remember, if $G=1$ and if observing from an angle of $\phi=\pm45°$, the undisturbed motion represents an extensional flow (see figure 2). From the literature, we are familiar with the fact that extensional flow is much more effective than simple shear flow in terms of drop deformation and breakup. This is also reflected from (5.5) and (5.6), where larger deformations are expected when $G=1$ than

https://doi.org/10.1017/jfm.2026.11819 Published online by Cambridge University Press

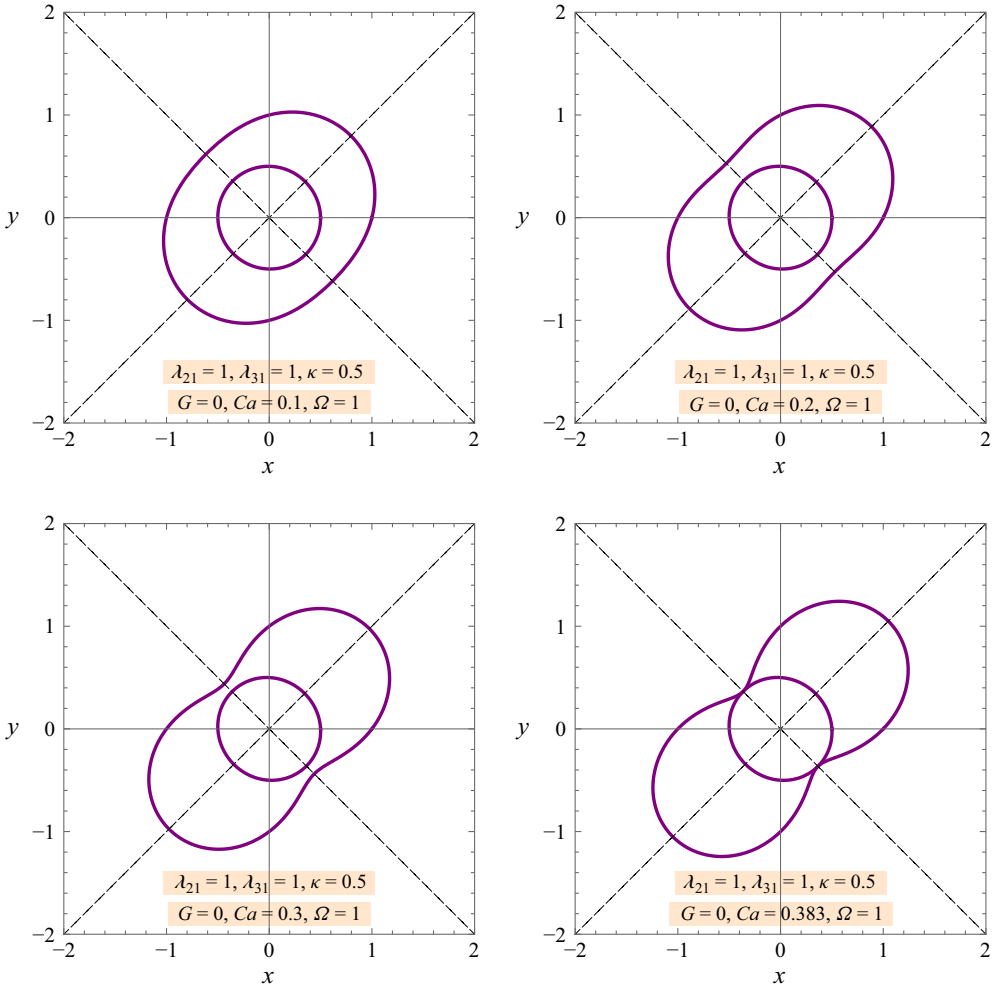


Figure 8. Deformation of a double emulsion droplet with $\lambda_{21} = 1$, $\lambda_{31} = 1$, $\kappa = 1/2$, $G = 0$ and $\Omega = 1$, as a function of Ca.

when $G = 0$. Indeed, the same observations found in figure 8 are relevant to figure 9, except of the fact that these occur at smaller capillary numbers. Here, the $R_{21} = R_{32}$ breakup mechanism is at $Ca = 15\,653/81\,830 = 0.191$, exactly half of that found in figure 8.

Up to now, we explored deformations with zero or positive flow-type parameters ($G = 0$ and $G = 1$), leading to the obvious next case of $G = -1$. However, if $G = -1$, the undisturbed motion suggests a clockwise rotation with no angular deformation (see figure 2). As a result, no deformation is possible for the case $G = -1$, regardless of the value of Ca, as it is reflected by (5.5) and (5.6). In figure 10, we continue to explore the influence of Ca on the same double emulsion droplet of figures 8 and 9 ($\lambda_{21} = 1$, $\lambda_{31} = 1$, $\kappa = 1/2$, $\Omega = 1$), but the flow-type parameters chosen are $G = -0.5$ and $G = -2$. As expected, the deformation increases with an increase of Ca. In the first two cases of figure 10 ($G = -0.5$), the inclination of the major axes of the outer and inner surfaces are as before at $\phi = +45°$ and $\phi = -45°$, respectively. The opposite is found when $G = -2$. Here, the inclination of the major axis of the outer surface is at $\phi = -45°$, while that of the inner surface is at $\phi = +45°$.

https://doi.org/10.1017/jfm.2026.11819 Published online by Cambridge University Press

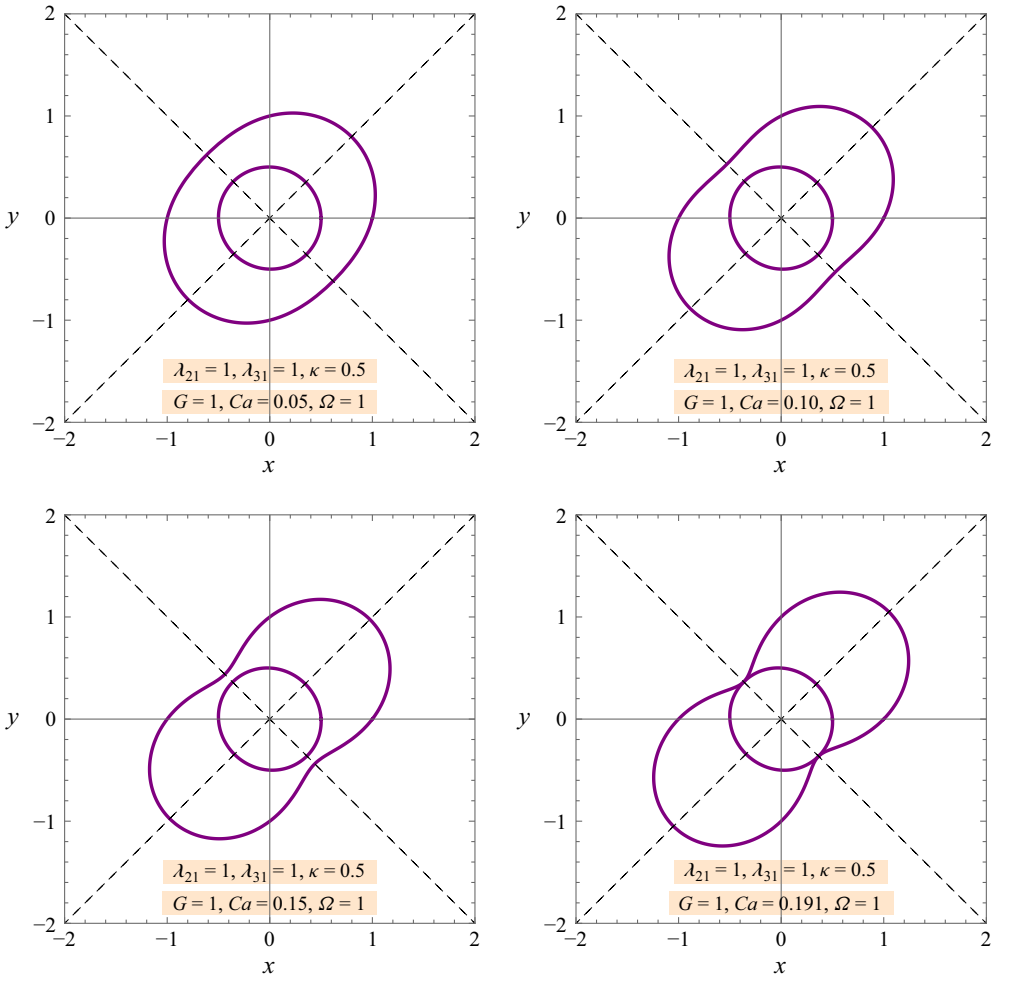


Figure 9. Deformation of a double emulsion droplet with $\lambda_{21} = 1$, $\lambda_{31} = 1$, $\kappa = 1/2$, $G = 1$ and $\Omega = 1$, as a function of Ca.

So far, we encounter with one (unofficial) breakup mechanism in which the outer surface (R_{21}) touches the inner surface (R_{32}). This occurs at $\phi = \pm 45^\circ$ and is only possible for $G \neq 1$. Substituting this azimuth angle in the xy plane ($\eta = 0$) results in an expression for this critical capillary number. An approximate expression for the $R_{21} = R_{32}$ breakup point can be obtained in the form of a Taylor series for the radii ratio (κ) around $\kappa = 0$. The leading terms read

$$Ca_{cr} = \pm \frac{1}{(1+G)} \frac{16\,(1+\lambda_{21})}{(16+19\lambda_{21})}\,(1-\kappa)\,, \tag{5.7}$$

where λ_{31} appears in the next term which is $O(\kappa^3)$ and Ω comes out starting from the $O(\kappa^4)$ term. Here, the plus or minus sign needs to be chosen by the reader depending on the orientation of the drop which depends on the flow-type parameter G. For the double emulsion droplet in figures 8 and 9 ($\lambda_{21} = 1$, $\lambda_{31} = 1$, $\kappa = 1/2$, $\Omega = 1$), this approximation suggests $Ca_{cr} = 0.457$ for $G = 0$ and $Ca_{cr} = 0.229$ for $G = 1$, compared with the exact values of $Ca_{cr} = 0.383$ for $G = 0$ and $Ca_{cr} = 0.191$ for $G = 1$. Clearly, this approximation

https://doi.org/10.1017/jfm.2026.11819 Published online by Cambridge University Press

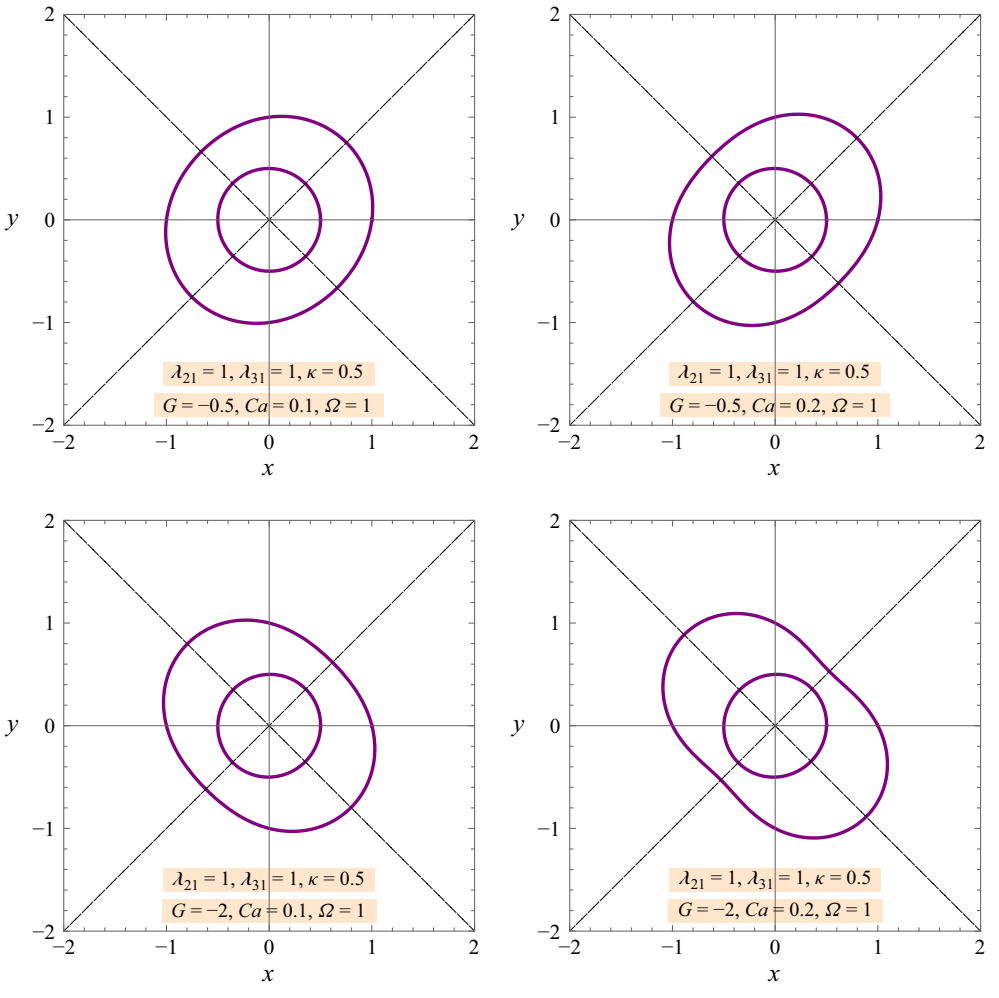


Figure 10. Deformation of a double emulsion droplet with $\lambda_{21} = 1$, $\lambda_{31} = 1$, $\kappa = 1/2$ and $\Omega = 1$, as a function of Ca. Upper panels: $G = -0.5$, lower panels: $G = -2$.

can be improved by considering more terms in the Taylor series. Note that (5.7) predicts no breakup when $G = -1$ in accordance with our previous explanation. A similar treatment for the $R_{21} = R_{32}$ breakup mechanism, but around $\kappa \to 1$, results in the following leading term:

$$Ca_{cr} = \pm \frac{16\Omega}{5\,(1+G)\,(1+\Omega)}\,(1-\kappa)^2\,, \tag{5.8}$$

where λ_{21}, λ_{31} start to appear in the next term of $O[(1-\kappa)^3]$. For a double emulsion droplet with $\lambda_{21} = 1$, $\lambda_{31} = 1$, $\kappa = 0.9$, $G = 0$ and $\Omega = 1$, this simple approximation results in $Ca_{cr} = 0.016$, which is closed to exact value of $Ca_{cr} = 0.0175$.

A second type of (unofficial) breakup mechanism has been suggested by Stone & Leal (1990) in their study of a double emulsion droplet in an extensional flow. In this mechanism, the inner drop breaks, while the shell fluid remains continuous. We shall call it the $R_{32} = 0$ breakup mechanism. Substituting $R_{32} = 0$ at $\phi = \pm 45°$ and performing a Taylor series, for κ, around $\kappa = 0$, results in the following leading term:

https://doi.org/10.1017/jfm.2026.11819 Published online by Cambridge University Press

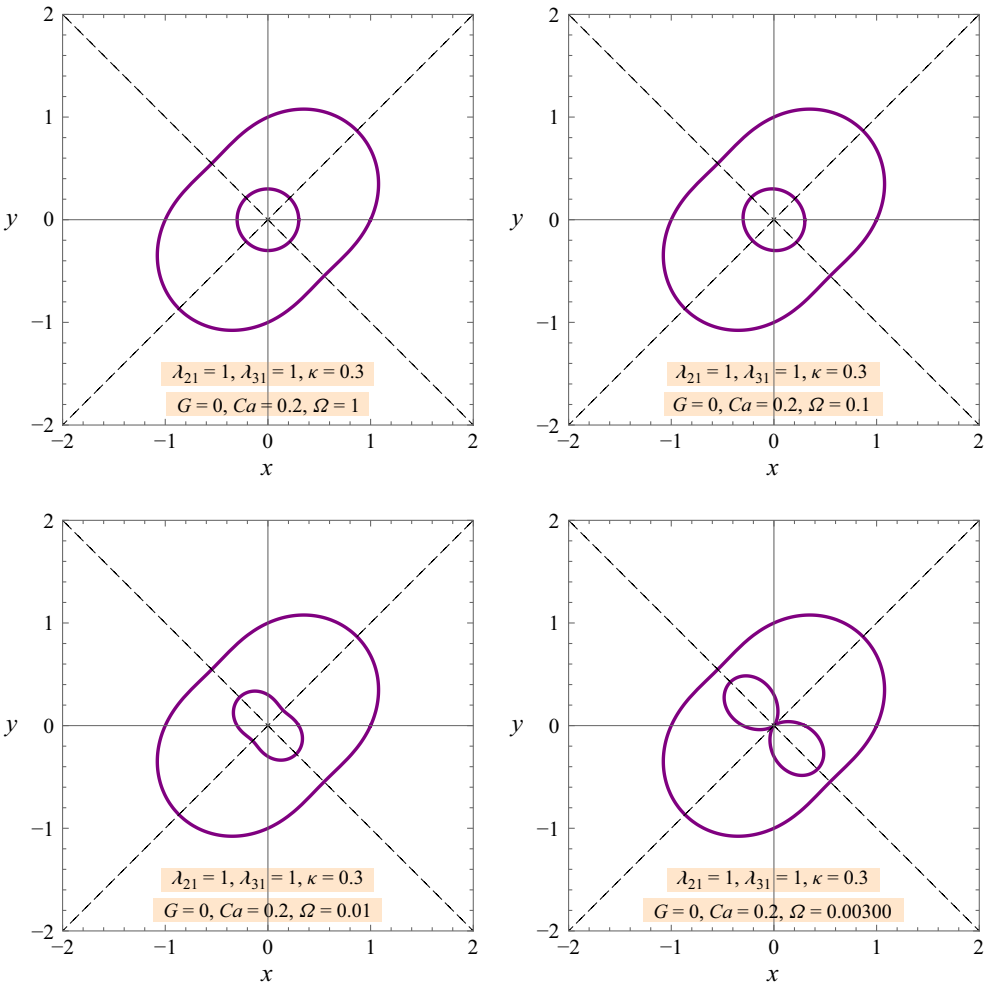


Figure 11. Deformation of a double emulsion droplet with $\lambda_{21}=1$, $\lambda_{31}=1$, $\kappa=0.3$, $G=0$ and $Ca=0.2$, as a function of Ω.

$$Ca_{cr}=\pm\frac{16\Omega}{(1+G)}\frac{(1+\lambda_{21})\,(\lambda_{21}+\lambda_{31})}{\lambda_{21}\,(16\lambda_{21}+19\lambda_{31})}\frac{1}{\kappa^3}. \tag{5.9}$$

According to (5.9), the most effective way to do so (breakup at smaller Ca) is by reducing the surface tension of the inner surface (σ_{32}), which is equivalent to reduce the value of Ω.

Figure 11 shows the process of reducing Ω in a double emulsion droplet with $\lambda_{21}=1$, $\lambda_{31}=1$, $\kappa=0.3$, $G=0$ and $Ca=0.2$. In the first two cases ($\Omega=1$, $\Omega=0.1$), the outer surface (R_{21}) is more deformed than the inner surface (R_{32}). This changes in the third case ($\Omega=0.01$), where the opposite occurs and the familiar peanut shape is developed, also in the inner surface. Finally, when $\Omega=0.00300$, the $R_{32}=0$ breakup mechanism is developed. Clearly, in the last case, the small deformation analysis performed here breaks down completely and, therefore, one should take the numerical values with great care. Nevertheless, we believe that as a qualitative analysis, it is correct. For the last double emulsion droplet in figure 11, (5.9) suggests $Ca_{cr}=0.203$ compared with the $O(Ca^1)$ exact value of $Ca_{cr}=0.200$. Clearly, that (5.9) predicts no $R_{32}=0$ breakup mechanism when

https://doi.org/10.1017/jfm.2026.11819 Published online by Cambridge University Press

$G=-1$ as deformation in this case is not possible. An approximate expression for the $R_{32}=0$ breakup mechanism, around $\kappa=1$, results in

$$Ca_{cr}=\pm\frac{16\Omega}{5\,(1+G)}\,(1-\kappa)\,, \tag{5.10}$$

where λ_{21}, λ_{31} appear in the next term of $O[(1-\kappa)^2]$. For most practical purposes, $\Omega\sim 1$, and the $R_{21}=R_{32}$ breakup mechanism will always occur first, notably when $\kappa\to 1$.

For organic liquids, the surface tension is typically $\sigma\approx 20$–$30\ \mathrm{mN\,m^{-1}}$, while for water, it is $\sigma\approx 70\ \mathrm{mN\,m^{-1}}$. Therefore, regardless of how the double emulsion is formulated, we obtain $\Omega\sim 1$. Adding surfactants mainly reduces the surface tension of water, but does not change the fact that $\Omega\sim 1$. Consequently, we conclude that the $R_{32}=0$ breakup mechanism is probably not relevant for the systems studied here.

Once again, the two breakup mechanisms presented here are based on geometrical criteria and do not represent the actual breakup points, which correspond to a transient and unstable state. Therefore, the breakup phenomenon described here should be interpreted as a qualitative result.

We conclude this chapter by introducing the Taylor deformation parameter (Taylor 1934) as a measurement of the deformation degree. For a double emulsion droplet, we have two of them: D_{21} and D_{32} for the outer and inner interfaces, respectively. Let $L_{ij}=R_{ij,max}$ and $B_{ij}=R_{ij,min}$ be the major and minor semi-axes ($ij=21$, 32), aligned at $\phi=\pm 45^\circ$. Then, by applying a Taylor series for the radii ratio (κ) around $\kappa=0$, the following approximated expressions can be obtained:

$$\begin{aligned} D_{21}&=\frac{L_{21}-B_{21}}{L_{21}+B_{21}}\\ &=\left|Ca\,(1+G)\,\frac{(16+19\lambda_{21})}{16\,(1+\lambda_{21})}\left[1+\frac{3\lambda_{21}\,(19+16\lambda_{21})\,(2\lambda_{21}+5\lambda_{31})}{4\,(1+\lambda_{21})\,(16+19\lambda_{21})\,(\lambda_{21}+\lambda_{31})}\kappa^3\right]\right|, \end{aligned} \tag{5.11}$$

$$D_{32}=\frac{L_{32}-B_{32}}{L_{32}+B_{32}}=\left|\frac{Ca}{\Omega}\,(1+G)\,\frac{\lambda_{21}\,(16\lambda_{21}+19\lambda_{31})}{16\,(1+\lambda_{21})\,(\lambda_{21}+\lambda_{31})}\kappa^3\right|. \tag{5.12}$$

Note that $D_{ij}=0$ suggests a sphere and $D_{ij}\to 1$ a slender interface. We also included the absolute value for the Taylor deformation parameter to be always positive. When $\kappa\to 0$, the double emulsion droplet becomes a single drop, D_{21} reduces to the familiar expression in the literature and $D_{32}=0$. Once again, when $G=-1$, no deformation is possible and $D_{21}=D_{32}=0$.

The two Taylor deformation parameters for a double emulsion droplet with $\lambda_{21}=1$, $\lambda_{31}=1$ and $\Omega=1$, as a function of the capillary number, for different values of κ and G, are presented in figure 12. In this figure we show the exact $O(Ca^1)$ solution and not the approximations in (5.11) and (5.12). For all cases, $D_{21}>D_{32}$, that is, the outer interface is more elongated than the inner interface, and as κ increases, both D_{21} and D_{32} increase. The solid circles are placed at the $R_{21}=R_{32}$ breakup point, suggesting that as κ increases, this mechanism is obviously facilitated (smaller critical Ca). Since $\Omega=1$, the $R_{32}=0$ breakup mechanism is not achievable and for most practical cases, and the $R_{21}=R_{32}$ breakup mode will occur first.

https://doi.org/10.1017/jfm.2026.11819 Published online by Cambridge University Press

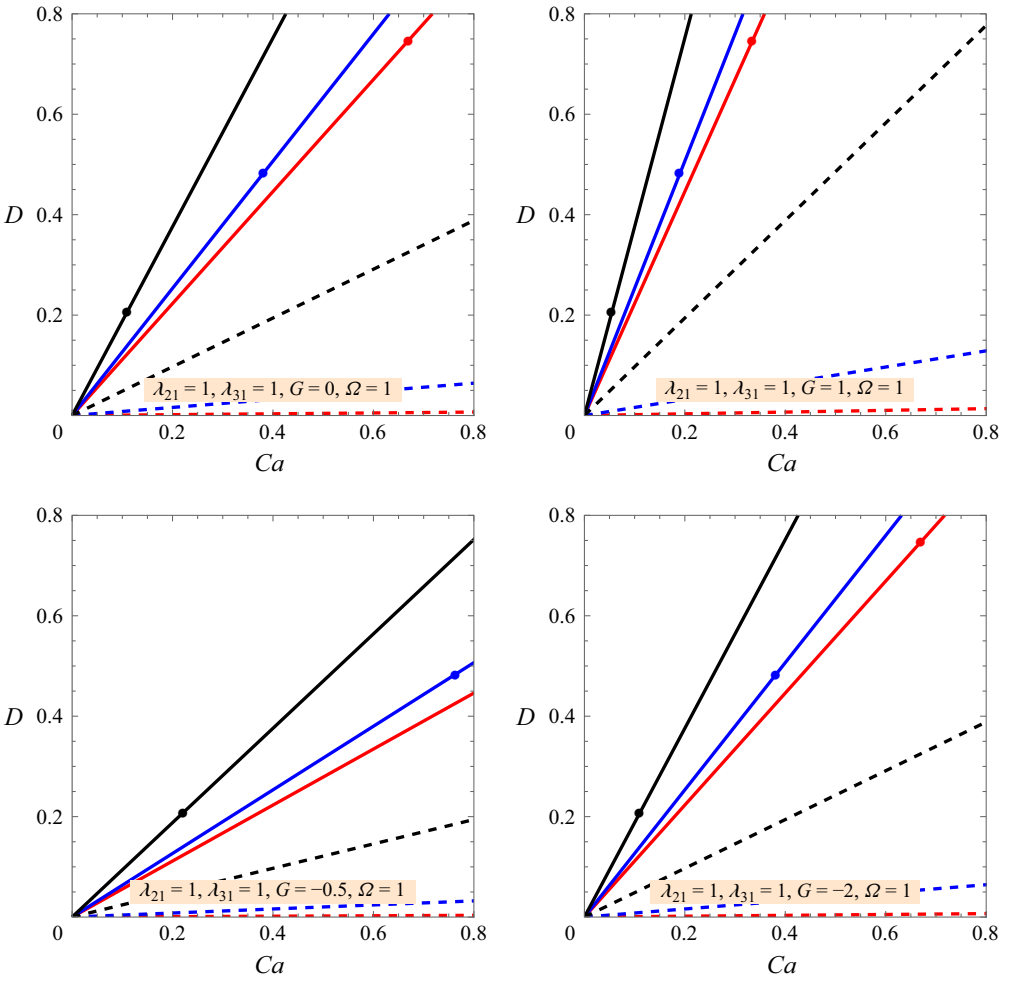


Figure 12. Taylor deformation parameters, for a double emulsion droplet with $\lambda_{21} = 1$, $\lambda_{31} = 1$ and $\Omega = 1$, as a function of Ca, for different values of κ and G. Solid lines, D_{21}; dashed lines, D_{32}. Black, $\kappa = 0.75$; blue, $\kappa = 0.50$; red, $\kappa = 0.25$. Solid circles, $R_{21} = R_{32}$ breakup mechanism.

6. Effective viscosity of a dilute double emulsion

We can now apply the $O(Ca^0)$ solution, developed in § 3, to determine the effective viscosity of a dilute emulsion containing spherical double emulsion droplets. Our discussion here follows the treatments presented by Batchelor (1970), Stone & Leal (1990) and Taylor (1932), who extended the works of Einstein (1906, 1911). Consider a dilute emulsion containing spherical double emulsion droplets which behaves like a Newtonian fluid with an effective viscosity (μ_{eff}). According to the above-mentioned literature, μ_{eff} is a linear function of the spherical droplets volume fraction (Φ) and depends only on the constant $b1_{-3,2}$ in (4.1) of the external fluid:

$$\frac{\mu_{eff}}{\mu_1} = 1 + \left| \frac{3}{(1+G)} b1_{-3,2} \right| \Phi$$
$$= 1 + \left[\frac{10H_1\lambda_{21}{}^2 + (1-\kappa)^2\, H_2\lambda_{31} + H_3\lambda_{21}\,(2+5\lambda_{31})}{4H_1\lambda_{21}{}^2 + (1-\kappa)^2\, H_2\lambda_{31} + 2H_3\lambda_{21}\,(1+\lambda_{31})} \right] \Phi, \qquad (6.1)$$

https://doi.org/10.1017/jfm.2026.11819 Published online by Cambridge University Press

where the coefficients H_1, H_2 and H_3, are functions of κ only, and are listed in the Appendix A. For the simple case of equal viscosities everywhere, $\lambda_{21}=1$, $\lambda_{31}=1$, we have

$$\frac{\mu_{eff}}{\mu_1}=1+\frac{14\left(2+4\kappa+6\kappa^2+3\kappa^3\right)}{\left(16+32\kappa+48\kappa^2+15\kappa^3-18\kappa^4-9\kappa^5\right)}\Phi. \tag{6.2}$$

Equation (6.2) is identical to the case of a double emulsion droplet in an axisymmetric extensional flow presented by Favelukis (2023), suggesting that the effective viscosity does not depend on G or on the type of the linear flow (simple shear flow, axisymmetric extensional flow, planar extensional flow, etc.).

Several asymptotic cases can be obtained by performing a Taylor series on (6.1) and we present here the two leading terms. When $\kappa\to 0$, the inner drop is very small and we get

$$\frac{\mu_{eff}}{\mu_1}=1+\frac{(2+5\lambda_{21})}{2\,(1+\lambda_{21})}\left[1+\frac{9\lambda_{21}\,(2\lambda_{21}+5\lambda_{31})}{4\,(1+\lambda_{21})\,(2+5\lambda_{21})\,(\lambda_{21}+\lambda_{31})}\kappa^3\right]\Phi. \tag{6.3}$$

Note that when the double emulsion droplet becomes a single drop ($\kappa=0$), Taylor's expression is recovered. If the fluid shell is very viscous $\lambda_{21}\to\infty$:

$$\frac{\mu_{eff}}{\mu_1}=1+\frac{5}{2}\left(1-\frac{3H_3}{10H_1\lambda_{21}}\right)\Phi. \tag{6.4}$$

Thus, if the double emulsion droplet behaves like a solid particle ($\lambda_{21}=\infty$), Einstein's formula is obtained. According to Stone & Leal (1990), another way for the double emulsion droplet to behave like a solid particle is when the fluid shell is very thin or $\kappa\to 1$:

$$\frac{\mu_{eff}}{\mu_1}=1+\frac{5}{2}\left[1-\frac{(1-\kappa)}{\lambda_{21}}\right]\Phi. \tag{6.5}$$

Confirming that if $\kappa\to 1$, the double emulsion droplet mimics a solid particle, with Einstein's formula being recovered.

Figure 13 describes the influence of the radii ratio (κ) on the effective viscosity (μ_{eff}) of a dilute emulsion, containing spherical double emulsion droplets, with $\lambda_{21}=1$ and $\lambda_{31}=1$, according to (6.1). The smallest effective viscosity belongs to a single drop ($\kappa\to 0$) obeying Taylor's expression. As κ increases, μ_{eff} also increases, until the upper limit of a very thin shell ($\kappa\to 1$) is reached, where μ_{eff} corresponds to Einstein's formula.

In figure 14, we describe the influence of the viscosity ratio λ_{21} on the effective viscosity of a dilute emulsion, containing spherical double emulsion droplets, having $\lambda_{31}=1$ and $\kappa=0.5$, according to (6.1). The smallest effective viscosity is for an inviscid shell fluid ($\lambda_{21}=0$). Here, μ_{eff} does not depend on λ_{31} or κ, and its value is the lowest possible one according to Taylor's expression ($1+\Phi$). The upper limit corresponds to a very viscous shell fluid ($\lambda_{21}\to\infty$) where, once again, μ_{eff} does not depend on λ_{31} or κ, and the emulsion behaves like a suspension with an effective viscosity according to the formula of Einstein.

7. Deformation of a double emulsion droplet with a highly viscous shell

For the case of a single drop, Taylor (1932, 1934) and later others distinguished between two types of small deformations regimes: $Ca\ll 1$, $\lambda=O(1)$ and $Ca=O(1)$, $\lambda\gg 1$. In § 5, we extended Taylor's theory to the case of a double emulsion droplet for the first regime only and we shall now make an attempt to deal with the second one. According to Taylor (1934), a single very viscous drop ($\lambda\gg 1$) in a simple shear flow ($G=0$) remains spherical, even at $Ca=O(1)$, if the external flow has sufficient vorticity. In this case, the

https://doi.org/10.1017/jfm.2026.11819 Published online by Cambridge University Press

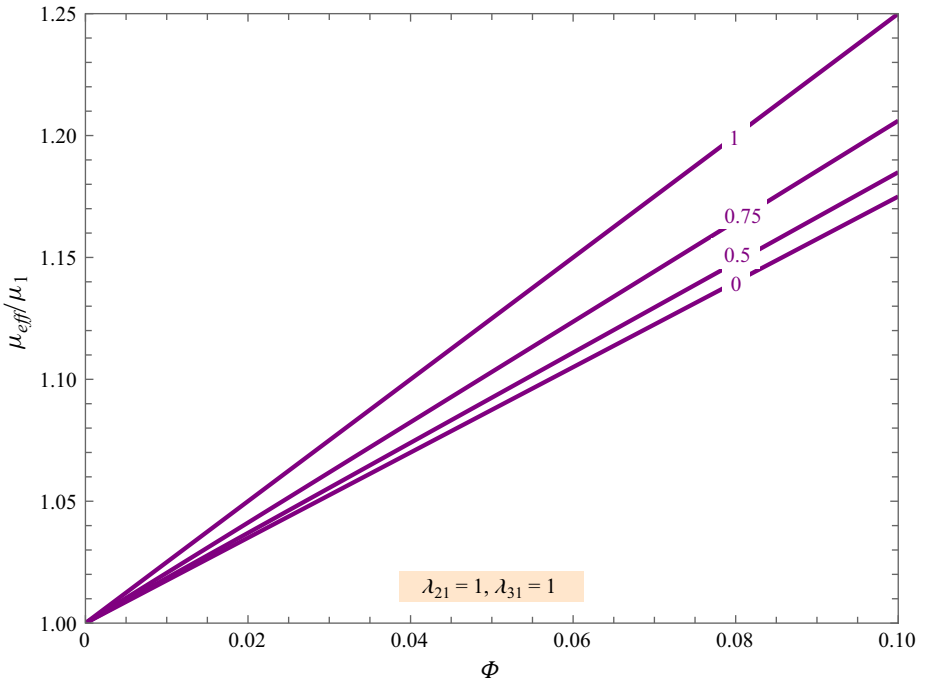


Figure 13. The effective viscosity of a dilute emulsion containing spherical double emulsion droplets, with $\lambda_{21} = 1$ and $\lambda_{31} = 1$, as a function of Φ, for different values of κ.

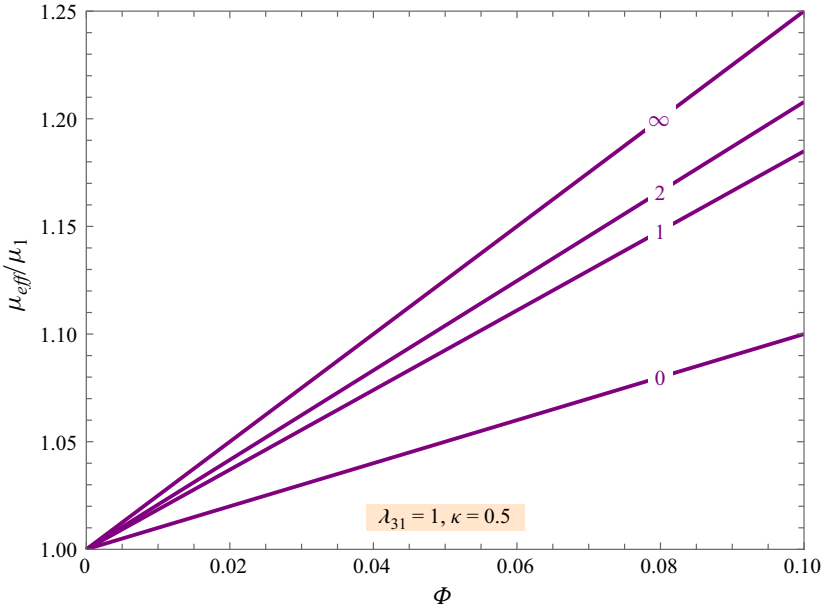


Figure 14. The effective viscosity of a dilute emulsion containing spherical double emulsion droplets, with $\lambda_{31} = 1$ and $\kappa = 0.5$, as a function of Φ, for different values of λ_{21}.

https://doi.org/10.1017/jfm.2026.11819 Published online by Cambridge University Press

drop is aligned with the direction of the flow at $\phi = 0°$ and it rotates almost as if it were a solid particle (Frankel & Acrivos 1970; Stone 1994). Applying the same arguments to the case of a double emulsion droplet, we might expect a similar behaviour when the viscosity of the shell is much greater than that of the external fluid: $\lambda_{21} \gg 1$ and for simplicity, we shall still demand $\lambda_{31} = O(1)$.

In this section, we closely follow the procedure of Taylor (1934), but adjust it to the present case. Let us repeat the $O(Ca^0)$ spherical solution in § 4, but with a few changes. In the outer surface (21) only, the normal velocities still remain continuous, yet they do not vanish. Instead, the normal stress balance in the outer surface, (2.43), is incorporated, with the right-hand side being changed to $2/Ca$. The situation in the inner surface (32) remains as before. That is, the normal velocities are continuous and equal to zero, and the normal stress balance, (2.44), does not participate in obtaining the $O(Ca^0)$ spherical solution. With the assistance of the Mathematica software, analytical expressions for a new set of constants were found ($b1_{-3,2}$, $d1_{-3,2}$, $b2_{-3,2}$, $d2_{-3,2}$, $b2_{2,2}$, $d2_{2,2}$, $e2_{1,0}$, $b3_{2,2}$, $d3_{2,2}$, $e3_{1,0}$), all of them being different than those in § 4, except of $e2_{1,0}$, $e3_{1,0}$ which remain as before. Once again, the rest of the other coefficients vanish.

Following Taylor (1934), we define the distance from the origin to the outer surface (21) of the double emulsion droplet, in the $z = 0$ ($\theta = \pi/2$, $\eta = 0$) plane, as follows:

$$R_{21}(\phi) = 1 + f_{21}(\phi). \tag{7.1}$$

The normal velocity and the azimuthal velocity at the outer surface are:

$$v_r = \frac{\mathrm{d}R_{21}}{\mathrm{d}t} = \frac{\mathrm{d}f_{21}}{\mathrm{d}t} = \frac{\mathrm{d}f_{21}}{\mathrm{d}\phi}\frac{\mathrm{d}\phi}{\mathrm{d}t}, \tag{7.2}$$

$$v_\phi = r\sin\theta\frac{\mathrm{d}\phi}{\mathrm{d}t} = \frac{\mathrm{d}\phi}{\mathrm{d}t}. \tag{7.3}$$

Note that the outer surface ($r = 1$) and the $z = 0$ plane ($\theta = 90°$) have been substituted into (7.3). By combining (7.2) and (7.3), an expression for the shape function can be suggested:

$$f_{21}(\phi) = \int \frac{v_r}{v_\phi}\,\mathrm{d}\phi. \tag{7.4}$$

Since, at first approximation, a two-dimensional mass balance must be conserved, we require that

$$\int_0^{2\pi} f_{21}\,\mathrm{d}\phi = 0. \tag{7.5}$$

In (7.2)–(7.4), v_r and v_φ are for the external fluid 1 or for the shell fluid 2, both at $r = 1$, under the assumption that the shell is very viscous, when compared with the external fluid or with the inner drop ($\lambda_{21} \gg 1$, $\lambda_{31} = O(1)$). As before, and to avoid a long and cumbersome presentation, we express the results as a Taylor series for the radii ratio (κ) around $\kappa = 0$. The leading terms of the outer surface, in the $z = 0$ plane, are

$$R_{21} = 1 + \frac{5(1+G)}{4(1-G)\lambda_{21}}\cos(2\phi)\left[1 - \frac{40}{19}\kappa^3\right]. \tag{7.6}$$

Note that the shape of the outer surface is independent of Ca and λ_{31}, but this is not the situation for the inner interface. For a single drop ($\kappa = 0$) in the familiar simple shear flow ($G = 0$) in the x-direction, (7.6) reduces to Taylor's (1934) result. Since we are dealing with small deformations ($f_{21} \ll 1$), (7.6) must be restricted to $\lambda_{21} \gg 1$, $Ca = O(1)$ and

https://doi.org/10.1017/jfm.2026.11819 Published online by Cambridge University Press

$G = O(1)$, and it is not valid for $G \to 1$. When $\lambda_{21} \gg 1$ and $G \to 1$, vorticity is absent in the flow, the outer surface does not rotate, $\boldsymbol{v}_\phi = 0$ and the previous treatment in § 4 still applies.

The shape of the inner surface (32) is treated as before according to the guidelines presented in § 5. If the result for the shape is further restricted to $\lambda_{21} \gg 1$ and $\lambda_{31} = O(1)$, then the leading two terms take then the form of

$$R_{32} = \kappa \left[1 + \frac{5}{3} \frac{Ca}{\Omega} (1 + G) \left(1 - \eta^2\right) \sin(2\phi) \kappa^3 \right]. \tag{7.7}$$

Since the inner surface must be a slightly deformed sphere, we require $G = O(1)$ and $Ca/\Omega \ll 1$.

Figure 15 describes the deformation of a double emulsion droplet, at the $z = 0$ plane, with $\lambda_{21} = 10$, $\lambda_{31} = 1$, $\kappa = 1/2$, $Ca = 1$ and $\Omega = 1$, for different values of G. The plot describes the exact solution and not the approximations given by (7.6) and (7.7). The first case is the familiar simple shear flow ($G = 0$) in the x-direction. Note that the outer surface (R_{21}) is less deformed than the inner surface (R_{32}). The major axis of R_{21} is at $\phi = 0°$, while the major axis of R_{32} is at $\phi = +45°$, a different behaviour than that shown in figure 8. Next is $G = -2$, since $G = -1$ predicts no deformation, as anticipated from (7.6) and (7.7). Here, the opposite occurs than the previous case. That is, the major axis of R_{21} is at $\phi = 90°$, while that of R_{32} is at $\phi = -45°$. Since the case $G = 1$ is singular, other positive values were chosen ($G = 0.5$, $G = 2$). They show relatively larger deformation in both surfaces. There is however a difference in the orientation of the major outer axis. For $G = 0.5$, it is with the x axis, while for $G = 2$, it is with the y axis.

8. Deformation of a double emulsion droplet with a highly viscous inner drop

In the previous section, we took advantage of the simplified procedure presented by Taylor (1934) to obtain the shape of a double emulsion droplet having a highly viscous shell: $\lambda_{21} \gg 1$, but $\lambda_{31} = O(1)$. In this section, we shall do the opposite. That is, to explore the behaviour of the double emulsion droplet with a highly viscous inner drop: $\lambda_{31} \gg 1$ and $\lambda_{21} = O(1)$.

Once again, we repeat the $O(Ca^0)$ spherical solution in § 4 as follows. The boundary condition at the outer surface (21) remains unchanged, the normal velocities are continuous and equal to zero, and the normal stress balance, (2.43), does not participate in obtaining the $O(Ca^0)$ solution. The inner surface (32) is modified according to the procedure of Taylor (1934). The normal velocities remain continuous, but do not vanish, and the normal stress balance, (2.44), is incorporated with the right-hand side being changed to $2\Omega/(\kappa Ca)$. A new set of constants are obtained ($b1_{-3,2}$, $d1_{-3,2}$, $b2_{-3,2}$, $d2_{-3,2}$, $b2_{2,2}$, $d2_{2,2}$, $e2_{1,0}$, $b3_{2,2}$, $d3_{2,2}$, $e3_{1,0}$), all of them being different than those in §§ 4 or 7, except of $e2_{1,0}$, $e3_{1,0}$ which, as usual, remain unchanged.

We repeat the mathematical procedure in § 7, but adjust it to the inner surface ($r = \kappa$) at the $z = 0$ plane ($\theta = 90°$). By doing so, (7.1)–(7.5) are being replaced by the following set:

$$R_{32}(\phi) = \kappa \left[1 + f_{32}(\phi)\right], \tag{8.1}$$

$$v_r = \frac{\mathrm{d}R_{32}}{\mathrm{d}t} = \kappa \frac{\mathrm{d}f_{32}}{\mathrm{d}t} = \kappa \frac{\mathrm{d}f_{32}}{\mathrm{d}\phi} \frac{\mathrm{d}\phi}{\mathrm{d}t}, \tag{8.2}$$

https://doi.org/10.1017/jfm.2026.11819 Published online by Cambridge University Press

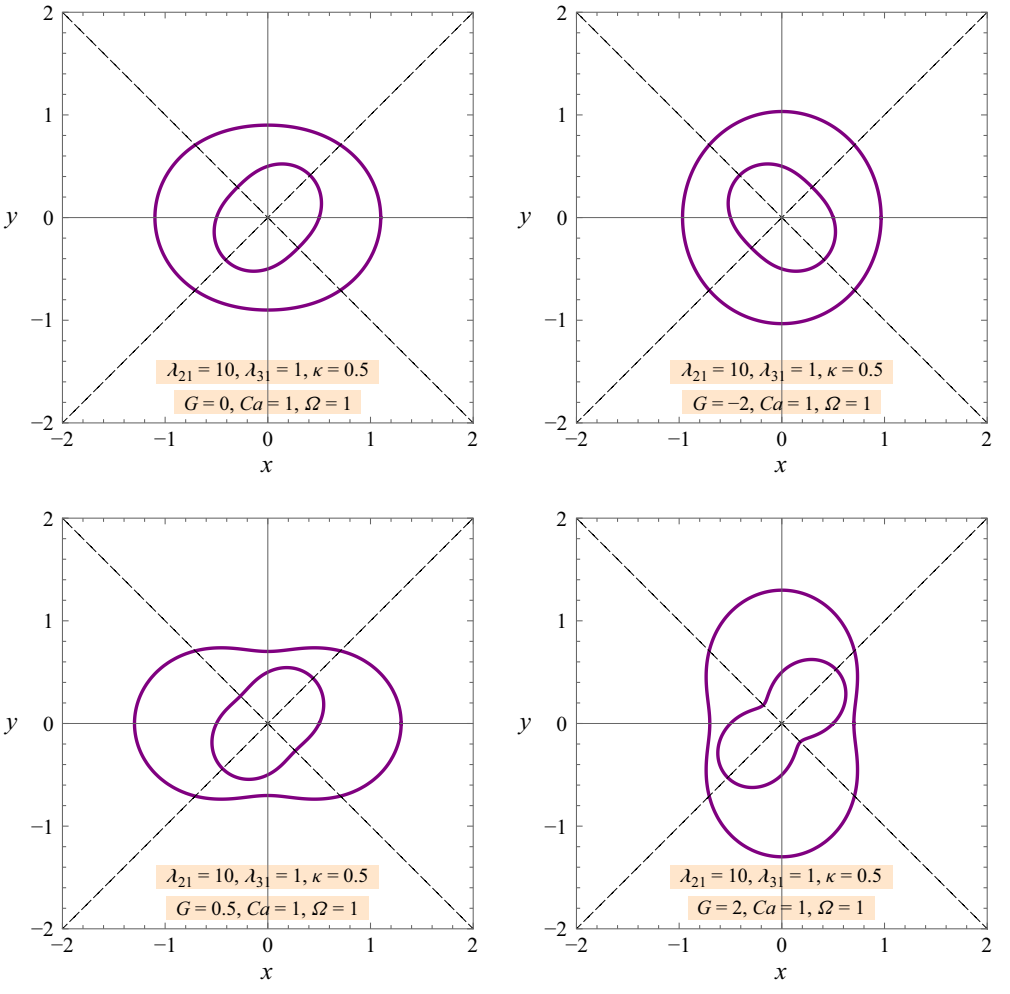


Figure 15. Deformation of a double emulsion droplet having a highly viscous shell with $\lambda_{21} = 10$, $\lambda_{31} = 1$, $\kappa = 1/2$, $Ca = 1$ and $\Omega = 1$, as a function of G.

$$v_\phi = r \sin\theta \frac{\mathrm{d}\phi}{\mathrm{d}t} = \kappa \frac{\mathrm{d}\phi}{\mathrm{d}t}, \tag{8.3}$$

$$f_{32}(\phi) = \int \frac{v_r}{v_\phi} \mathrm{d}\phi, \tag{8.4}$$

$$\int_0^{2\pi} f_{32} \, \mathrm{d}\phi = 0, \tag{8.5}$$

where in (8.4), v_r and v_φ belong to the shell fluid 2 or to the inner drop fluid 3, at $r = \kappa$, under the assumption that the inner drop is very viscous, when compared with the external fluid or to the shell fluid ($\lambda_{21} = O(1)$, $\lambda_{31} \gg 1$).

The shape of the outer surface (21) can be found according to the procedure presented in § 5 and that of the inner surface (32) according to this section. Applying a Taylor series for κ, around $\kappa = 0$, results in the following leading terms:

https://doi.org/10.1017/jfm.2026.11819 Published online by Cambridge University Press

$$R_{21} = 1 + Ca\,(1+G)\left(1-\eta^2\right)\sin(2\phi)\left[\frac{(16+19\lambda_{21})}{16\,(1+\lambda_{21})} + \frac{15\lambda_{21}\,(19+16\lambda_{21})}{64\,(1+\lambda_{21})^2}\kappa^3\right], \quad (8.6)$$

$$R_{32} = \kappa\left[1 - \frac{15}{8}\frac{(1+G)}{(1-G)}\frac{\lambda_{21}}{(1+\lambda_{21})\,\lambda_{31}}\cos(2\phi)\left(1-\frac{21}{19}\kappa^2\right)\right]. \quad (8.7)$$

Note that according to the slightly perturbed sphere approximation, the following conditions must be met: $\lambda_{21} = O(1)$, $\lambda_{31} \gg 1$, $G = O(1)$, but $G \neq 1$ and $Ca \ll 1$. The outer surface, (8.6), is the same as the one obtained in § 5, (5.5), after it is simplified according to $\lambda_{31} \gg 1$. Similar to § 7, where Ca did not enter in the expression for the outer surface, here, the modified capillary number of the inner surface (Ca/Ω) is absent in (8.7).

In figure 16, we explore the deformation of a double emulsion droplet with a highly viscous inner drop, at the $z=0$ plane, with $\lambda_{21}=1$, $\lambda_{31}=10$, $\kappa=1/2$ and $Ca=0.1$, for the same values of G as in figure 15. The figure describes the exact solution and not the approximations given by (8.6) and (8.7). We note that the major axis of R_{21} is at $\phi=\pm45°$, while the major axis of R_{32} is at $\phi=0°$ or $\phi=90°$, an opposite situation to that described in figure 15.

9. Conclusions

The report presented here explored the behaviour of a double emulsion droplet subjected to a two-directional shear flow under creeping flow conditions. The double emulsion droplet, which is submerged in an external fluid (fluid 1), is originally made up from a spherical inner drop (fluid 3) covered by a spherical fluid shell (fluid 2). The problem presented here is described by six dimensionless parameters, these are: the external capillary number (Ca); two viscosity ratios, shell over external (λ_{21}) and internal over external (λ_{31}); the radii ratio, inner over outer (κ); the surface tensions ratio, inner-shell over outer-shell (Ω); and the flow-type parameter (G).

First, we explored the undisturbed motion, that is, the flow in the absence of the double emulsion droplet, given in a dimensionless form as: $v_x = y$ and $v_y = Gx$. The case $G=0$ represents the familiar simple shear flow in the x-direction only with both angular deformation and rotation. When $G=\infty$, we have once again a simple shear flow, but this time, in the y-direction. If $G=1$, there is only angular deformation and if $G=-1$, there is rotation only.

Next, we took advantage of Lamb's general solution to the Stokes equations, and obtained analytical expressions for the external, shell and inner drop motions, under the assumption of a spherical double emulsion droplet ($Ca=0$, $\Omega=\infty$). Here, the problem is governed by four parameters only (λ_{21}, λ_{31}, κ, G) and we explored in detail the influence of each of them. In a simple shear flow in the x-direction ($G=0$), the following interesting observations in the $z=0$ plane were obtained: (a) the inviscid shell ($\lambda_{21}=0$) is the only case with open external streamlines, with an inner drop fluid rotating at an angular velocity of $\omega=-1/2$; (b) for a solid shell ($\lambda_{21}=\infty$), the shell and the inner drop fluids rotate, once again, at $\omega=-1/2$; (c) an internal solid sphere ($\lambda_{31}=\infty$) also rotates at $\omega=-1/2$; (d) in the limit of a very thin shell ($\kappa\to1$), both the shell and the inner drop behave like solids rotating at $\omega=-1/2$; (e) when $\lambda_{21}<1/2$, two additional stagnation points in the shell are sometimes possible, when compared with a single drop ($\kappa=0$). We also explored the influence of the flow-type parameter (G). When $G=1$ and from a $\phi=\pm45°$ point of view, we have an extensional flow. However, when $G=-1$, there is a clockwise rotation with $\omega=-1$ in all three fluids and the presence of the double emulsion droplet does not alter the undisturbed motion.

https://doi.org/10.1017/jfm.2026.11819 Published online by Cambridge University Press

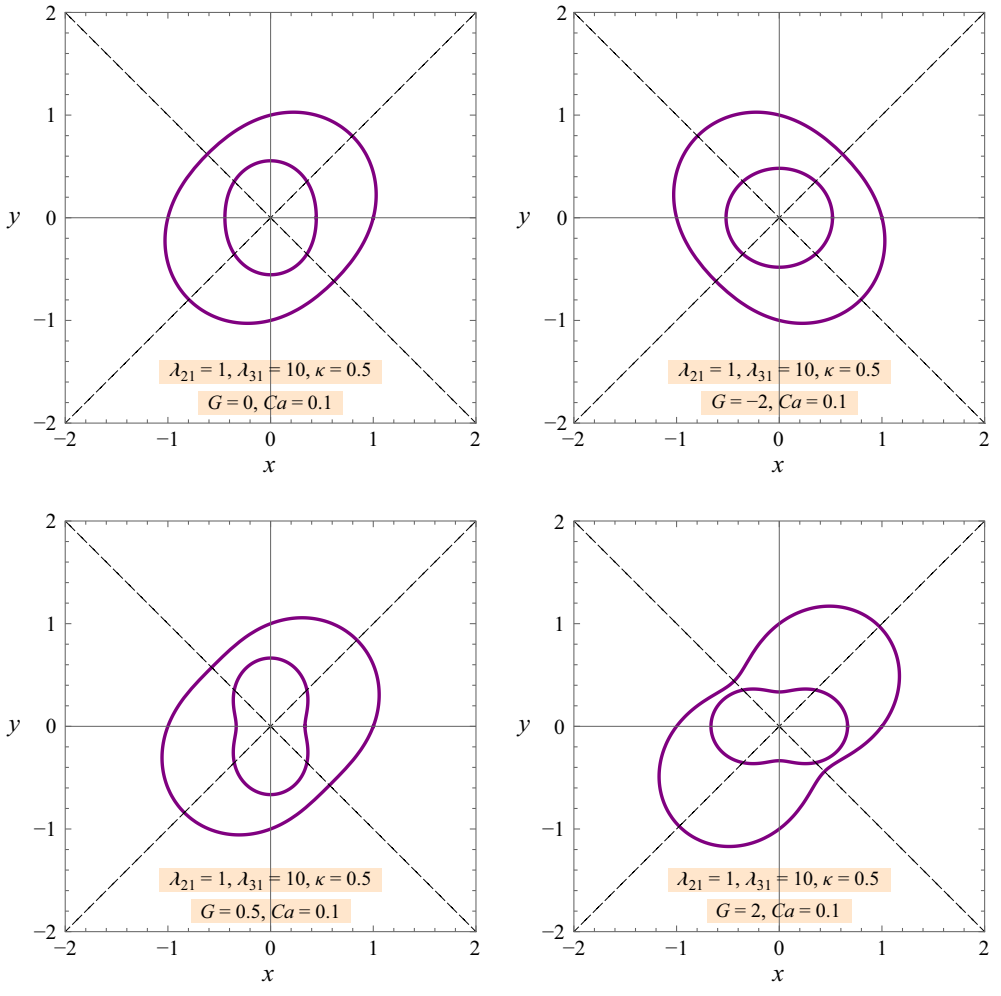


Figure 16. Deformation of a double emulsion droplet having a highly viscous inner drop with $\lambda_{21} = 1$, $\lambda_{31} = 10$, $\kappa = 1/2$, $Ca = 0.1$ and $\Omega = 1$, as a function of G.

We also considered a dilute emulsion, containing spherical double emulsion droplets, and obtained an analytical expression for the effective viscosity of such emulsion. In general, as the inner drop increases or as the shell decreases (as κ increases), or as the viscosity of the shell (λ_{21}) increases, the effective viscosity also increases. Several asymptotic expressions can be derived: (a) when the double emulsion droplet becomes a single drop ($\kappa = 0$), Taylor's expression is recovered; (b) if the double emulsion droplet behaves like a solid particle ($\lambda_{21} = \infty$), Einstein's formula is obtained; (c) when the fluid shell is very thin ($\kappa \to 1$), the double emulsion droplet mimics a solid particle and Einstein's formula is recovered.

We explored the small deformation of the double emulsion droplet under the following restrictions: $\lambda_{21} = O(1)$, $\lambda_{32} = O(1)$, $G = O(1)$, $Ca \ll 1$ and $Ca/\Omega \ll 1$. For a simple shear flow in the x-direction ($G = 0$), the outer surface is oriented at an azimuth angle $\phi = +45°$, while the inner surface is aligned at $\phi = -45°$. At relative very low capillary numbers (Ca), both surfaces are ellipsoids. As Ca increases, the deformation increases and at higher Ca, the surfaces attain a peanut shape. A similar behaviour was obtained when

https://doi.org/10.1017/jfm.2026.11819 Published online by Cambridge University Press

$G = 1$, a case which if observing from a $\phi = \pm 45°$ point of view, represents an extensional flow. As expected, and in accordance with the single drop literature, for the same Ca, larger deformations have been obtained in extensional flow ($G = 1$) than in simple shear flow ($G = 0$). If the flow-type parameter is negative ($G < 0$), interesting observations have been found. When $G = -1$, no deformation is possible, regardless the value of Ca. When $G > -1$, the inclination of the major axes of the outer and inner surfaces are as before at $\phi = +45°$ and $\phi = -45°$, respectively. The opposite occurs when $G < -1$ and the inclination of the major axis of the outer surface is at $\phi = -45°$, while that of the inner surface is at $\phi = +45°$.

Following the guidelines of Stone & Leal (1990), two types of breakup mechanisms were detected. In the first one, called here as $R_{21} = R_{32}$, the outer surface (R_{21}) touches the inner surface (R_{32}). In the second one, referred as $R_{32} = 0$, the inner drop breaks while the surrounding shell remains continuous. However, since the second breakup mechanism requires extremely low surface tension ratios ($\Omega \ll 1$), it is probably not physically possible. Clearly, these critical points cannot be declared as the official breaking points, since drop breakup is a complicated transient unstable situation in which the steady and slightly deformed theory presented here cannot predict.

Taylor (1934) also found out that a single very viscous drop ($\lambda \gg 1$) in a simple shear flow ($G = 0$) remains almost spherical, even at $Ca = O(1)$, rotating almost as if it were a solid particle. He found out that the orientation of the single drop is at $\phi = 0°$ with the direction of the flow and its deformation is independent of Ca. We followed Taylor's simplified arguments and extended his results for two additional cases: (a) a double emulsion droplet with a highly viscous shell; and (b) a double emulsion droplet with a highly viscous inner drop. The first case, of a highly viscous shell, was restricted to $\lambda_{21} \gg 1$, $\lambda_{31} = O(1)$, $G = O(1)$, $G \neq 1$ and $Ca \ll 1$. Here, the outer surface (R_{21}) is independent of Ca and the orientation of its larger axis is at $\phi = 0°$ or $\phi = 90°$, while the inner surface (R_{32}) depends on Ca and the orientation of its larger axis is at $\phi = \pm 45°$. In the second case of a very viscous inner drop restricted to $\lambda_{21} = O(1)$, $\lambda_{31} \gg 1$, $G = O(1)$, $G \neq 1$ and $Ca \ll 1$, the opposite occurs. That is, the outer surface (R_{21}) depends on Ca and the orientation of its larger axis is at $\phi = \pm 45°$, while the inner surface (R_{32}) does not depend on Ca and the orientation of its larger axis is at $\phi = 0°$ or $\phi = 90°$.

Fluid mechanics studies of double emulsion droplets in rotating mixing devices, undergoing shear or extensional flows, are very important because of their many industrial applications. The results from double emulsion droplets, with their additional phase, show that sometimes they behave like a single drop and sometimes they can mimic a solid particle. The current report presents analytical expressions for many physical situations and, as a result, it is limited to small deformations. In the future, a numerical investigation is recommended to extend the deformation domain. This may lead to a better description ofthe inner and outer surfaces orientations, the breakup mechanisms as well as to confirm our analytical predictions.

Funding. This research was supported by Shenkar – College of Engineering and Design.

Declaration of interests. The author reports no conflict of interests.

Appendix A

The functions H_i, with $i = 1$–9, inside the coefficients of the solid harmonics, according to (4.1)–(4.10):

$$H_1 = 1 + 2\kappa + 3\kappa^2 + 3\kappa^3 + 3\kappa^4 + 3\kappa^5 + 3\kappa^6 + 2\kappa^7 + \kappa^8, \tag{A1}$$

https://doi.org/10.1017/jfm.2026.11819 Published online by Cambridge University Press

$$H_2 = 4 + 16\kappa + 40\kappa^2 + 55\kappa^3 + 40\kappa^4 + 16\kappa^5 + 4\kappa^6, \tag{A2}$$

$$H_3 = 2 + 4\kappa + 6\kappa^2 + 3\kappa^3 - 3\kappa^5 - 6\kappa^6 - 4\kappa^7 - 2\kappa^8, \tag{A3}$$

$$H_4 = 1 + \kappa + \kappa^2 + \kappa^3 + \kappa^4 + \kappa^5 + \kappa^6, \tag{A4}$$

$$H_5 = 5 + 5\kappa - 2\kappa^2 - 2\kappa^3 - 2\kappa^4 - 2\kappa^5 - 2\kappa^6, \tag{A5}$$

$$H_6 = 1 + \kappa + \kappa^2, \tag{A6}$$

$$H_7 = 2 + 2\kappa + 2\kappa^2 - 3\kappa^3 - 3\kappa^4, \tag{A7}$$

$$H_8 = 2 + 2\kappa + 2\kappa^2 + 2\kappa^3 + 2\kappa^4 - 5\kappa^5 - 5\kappa^6, \tag{A8}$$

$$H_9 = 3 + 9\kappa + 11\kappa^2 + 9\kappa^3 + 3\kappa^4. \tag{A9}$$

References

Acrivos, A. 1983 The breakup of small drops and bubbles in shear flows. *Ann. New York Acad. Sci.* **404**, 1–11.

Acrivos, A. 1990 Deformation and burst of single drops in shear flows. *AIP Conf.* **197**, 3–6.

Bartok, W. & Mason, S.G. 1958 Particle motion in sheared suspensions. **VII**. Internal circulation in fluid droplets (theoretical). *J. Colloid Sci.* **13**, 293–307.

Batchelor, G.K. 1970 The stress system in a suspension of force-free particles. *J. Fluid Mech.* **41** (1970), 545–570.

Bentley, B.J. & Leal, L.G. 1986 A computer-controlled four-roll mill for investigations of particle and drop dynamics in two-dimensional linear shear flows. *J. Fluid Mech.* **167**, 219–240.

Briscoe, B.J., Lawrence, C.J. & Mietus, W.G.P. 1999 A review of immiscible fluid mixing. *Adv. Colloid Interface Sci.* **81**, 1–17.

Chaithanya, K.V.S. & Sumesh, P.T. 2019 Dynamics and stability of a concentric compound particle - a theoretical study. *Soft Matt.* **15**, 7605–7615.

Chaithanya, K.V.S. & Sumesh, P.T. 2020 Deformation dynamics of an active compound particle in an imposed shear flow-a theoretical study. *J. Phys. D: Appl. Phys.* **53**, 314001.

Chen, Y., Liu, X. & Shi, M. 2013 Hydrodynamics of double emulsion droplet in shear flow. *Appl. Phys. Lett.* **102**, 051609.

Chen, Y., Liu, X., Zhang, C. & Zhao, Y. 2015*a* Enhancing and suppressing effects of an inner droplet on deformation of a double emulsion droplet under shear. *Lab on a Chip* **15**, 1255–1261.

Chen, Y., Liu, X. & Zhao, Y. 2015*b* Deformation dynamics of double emulsion droplet under shear. *Appl. Phys. Lett.* **106**, 141601.

Davis, A.M.J. & Brenner, H. 1981 Emulsions containing a third solid internal phase. *J. Engng Mech. Div. ASCE* **107**, 609–621.

Das, S., Mandal, S. & Chakraborty, S. 2020 Interfacial viscosity-dictated morpho-dynamics of a compound drop in linear flows. *Phys. Fluids* **32**, 062006.

Einstein, A. 1906 Eine neue bestimmung der moleküldimensionen. *Ann. Phys.* **19**, 289–306.

Einstein, A. 1911 Berichtigung zu meiner arbeit: eine neue bestimmung der moleküldimensionen. *Ann. Phys.* **34**, 591–592.

Favelukis, M. 2020 A compound drop in a nonlinear extensional flow. *Eur. J. Mech. B/Fluids* **83**, 114–129.

Favelukis, M. 2021*a* Mass transfer around a compound drop in an extensional flow. *Can. J. Chem. Engng* **99**, S800–S808.

Favelukis, M. 2021*b* Mass transfer around a double emulsion droplet in a uniform flow. *Eur. J. Mech. B/Fluids* **89**, 501–508.

Favelukis, M. 2022 A drop in a nonlinear shear flow. *J. Fluid Mech.* **941**, A50.

Favelukis, M. 2023 A triple emulsion droplet in an extensional flow. *Eur. J. Mech. B/Fluids* **102**, 1–9.

Frankel, N.A. & Acrivos, A. 1970 The constitutive equation for a dilute emulsion. *J. Fluid Mech.* **44**, 65–78.

Happel, J. & Brenner, H. 1983 *Low Reynolds Number Hydrodynamics*. Kluwer.

Hua, H., Shin, J. & Kim, J. 2014 Dynamics of a compound droplet in shear flow. *Intl J. Heat Fluid Flow* **50**, 63–71.

https://doi.org/10.1017/jfm.2026.11819 Published online by Cambridge University Press

JOHNOSON, R.E. & SADHAL, S.S. 1985 Fluid mechanics of compound multiphase drops and bubbles. *Annu. Rev. Fluid Mech.* **17**, 289–320.
KAN, H.-C., UDAYKUMAR, H.S., SHYY, W. & TRAN-SON-TAY, R. 1998 Hydrodynamics of a compound drop with application to leukocyte modeling. *Phys. Fluids* **10**, 760.
KAOUI, B., KRÜGER, T. & HARTING, J. 2013 Complex dynamics of a bilamellar vesicle as a simple model for leukocytes. *Soft Matt.* **9**, 8057–8061.
KIM, S. & DABIRI, S. 2017 Transient dynamics of eccentric double emulsion droplets in a simple shear flow. *Phys. Fluids* **2**, 104305.
KRAVCHENKO, I.V. & PATLAZHAN, S.A. 2009 Hydrodynamics structuring of viscous composite drop in a shear flow. *Dokl. Phys. Chem.* **427**, 155–158.
LAMB, H. 1945 *Hydrodynamics*, 6th edn. Dover publications.
LANDAU, L.D. & LIFSHITZ, E.M. 1987 *Fluid Mechanics*, 2nd edn. Pergamon Press.
LEVANT, M. & STEINBERG, V. 2014 Complex dynamics of compound vesicles in linear flow. *Phys. Rev. Lett.* **112**, 138106.
MANDAL, S., GHOSH, U. & CHAKRABORTY, S. 2016 Effect of surfactant motion and deformation of compound droplets in arbitrary unbounded Stokes flows. *J. Fluid Mech.* **803**, 200–249.
PATLAZHAN, S.A., KRAVCHENKO, I.V., BUDTOVA, T.V. & SULTANOV, V.G. 2014 Deformation behavior of a composite drop in a simple shear flow. *Dokl. Phys. Chem.* **454**, 8–11.
PATLAZHAN, S., VAGNER, S. & KRAVCHENKO, I. 2015 Steady-state deformation behavior of confined composite droplets under shear flow. *Phys. Rev. E* **91**, 063002.
POWER, H. 1993 Low Reynolds number deformation of compound drops in shear flows. *Math. Meth. Appl. Sci.* **16**, 61–74.
QU, X. & WANG, Y. 2012 Dynamics of concentric and eccentric compound droplets suspended in extensional flows. *Phys. Fluids* **24**, 123302.
RALLISON, J.M. 1984 The deformation of small viscous drops and bubbles in shear flows. *Annu. Rev. Fluid Mech.* **16**, 45–66.
SADHAL, S.S., AYYASWAMY, P.S. & CHUNG, J.N. 1997 *Transport Phenomena with Drops and Bubbles*. Springer-Verlag.
SINGEETHAM, P.K., CHAITHANYA, K.V.S. & THAMPI, S.P. 2021 Dilute dispersion of compound particles: deformation dynamics and rheology. *J. Fluid Mech.* **917** (A2), 1–47.
SMITH, K.A., OTTINO, J.M. & OLVERA DE LA CRUZ, M. 2004 Encapsulated drop breakup in shear flow. *Phys. Rev. Lett.* **93**, 204501.
STONE, H.A. 1994 Dynamics of drop deformation and breakup in viscous fluids. *Annu. Rev. Fluid Mech.* **26**, 65–102.
STONE, H.A. & LEAL, L.G. 1990 Breakup of concentric double emulsion droplets in linear flows. *J. Fluid Mech.* **211**, 123–156.
STROEVE, P. & VARANASI, P.D. 1984 An experimental study on double emulsion drop breakup in uniform shear flow. *J. Colloid Interface Sci.* **99**, 360–373.
TAYLOR, G.I. 1932 The viscosity of a fluid containing small drops of another fluid. *Proc. R. Soc. Lond. A* **138**, 41–48.
TAYLOR, G.I. 1934 The formation of emulsions in definable fields of flow. *Proc. R. Soc. Lond. A* **146**, 501–523.
TIRIBOCCHI, A., MONTESSORI, A., AIME, S., MILANI, M., LAURICELLA, M., SUCCI, S. & WEITZ, D. 2020 Novel nonequilibrium steady states in multiple emulsions. *Phys. Fluids* **32**, 017102.
VEERAPANNENI, S.K., YOUNG, Y.-N., VLAHOVSKA, P.M. & BLAWZDZIEWICZ, J. 2011 Dynamics of a compound vesicle in shear flow. *Phys. Rev. Lett.* **106**, 158103.
VU, T.V., VU, L.V., PHAM, B.D. & LUU, Q.H. 2018 Numerical investigation of dynamic behaviour of a compound drop in shear flow. *J. Mech. Sci. Technol.* **32**, 2111–2117.
WANG, J., XU, S., HUANG, Y. & GUAN, J. 2018 Mechanical mechanisms of the directional shift and inverse of the eccentric compound droplet. *Phys. Fluids* **30**, 042005.
ZAPRYANOV, Z. & TABAKOVA, S. 1999 *Dynamics of Bubbles, Drops and Rigid Particles*. Kluwer Academic Publishers.

https://doi.org/10.1017/jfm.2026.11819 Published online by Cambridge University Press